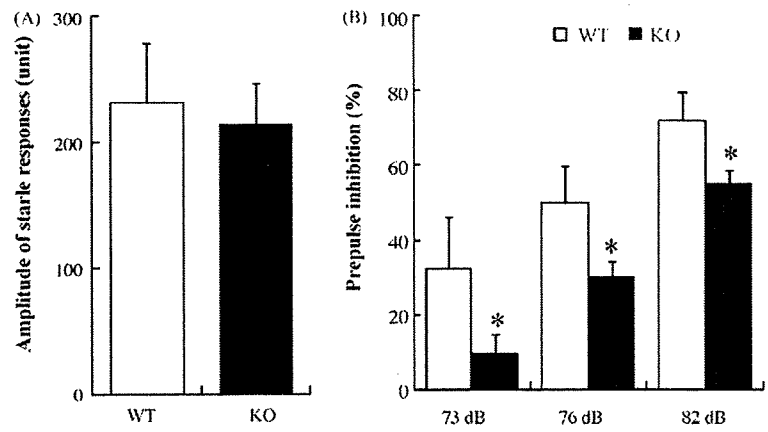

Fig. 3. Prepulse-inhibition (PPI) of acoustic startle response in WT and KO mice. (A) In the 120 dB-pulse-only trials, startle amplitude did not differ significantly between MT-3 KO and WT mice. (B) The PPI is expressed as a percentage of the startle response to a 120 dB-pulse. MT-3 KO mice showed diminished PPI at prepulse intensities of 73, 76, and 82 dB (vs. WT mice) ($p < 0.05$, t-test), $n = 15$ (WT), $n = 17$ (KO).

Data are presented as the means ± S.E.M. Statistical comparisons were made using a one-way ANOVA followed by a Student's t-test using Statview version 5.0 (SAS Institute Inc., Cary, NC, USA), with $p < 0.05$ being considered to indicate statistical significance.

In the locomotor activity test, MT-3 KO mice displayed a normal circadian rhythm (Fig. 1A). There was no significant difference between MT-3 KO and WT mice at any time point. In locomotor activity counts during the light phase, dark phase, and over 24 h (total), there was no significant difference between WT and KO mice (Fig. 1B). To examine the ability of habituation, we analyzed behavior during the first 3 h, but there was no difference (Fig. 1C).

To assess the social affiliative behavior of MT-3 KO mice, we employed a social interaction test. During a 10-min social-interaction test in a novel environment, there was no significant difference between MT-3 KO and WT mice regarding number of contacts (WT vs. KO: 30.7 ± 3.2 vs. 36.4 ± 2.9, $n = 11$) and total duration of contacts (WT vs. KO: 57.9 ± 10.1 vs. 47.3 ± 5.6, $n = 11$). But the mean duration per contact of MT-3 KO mice was significantly shorter than that of WT mice ($p < 0.05$, t-test) (Fig. 2).

To investigate the possible role of MT-3 in sensorimotor gating, PPI was measured. In the pulse-only trials, startle amplitude did not differ significantly between MT-3 KO and WT mice (Fig. 3 A). MT-3 KO mice showed diminished PPI at all prepulse intensities (vs. WT mice) ($p < 0.05$, t-test) (Fig. 3 B).

Erickson et al. have reported that MT-3 deficient mice exhibited normal learning and memory [4]. However, they did not show any results of other behavioral tests. Hence, in the present study, we investigated other behavioral tests evaluating schizophrenia-like behavior of MT-3 KO mice. MT-3 KO mice exhibited normal spontaneous locomotor activity, but abnormal social interaction and prepulse inhibition.

MT-3 exists in the CNS, but it is strongly induced in reactive astrocytes by brain stab wound, cerebral ischemia, and injection of kainic acid [12]. MT-3 has neuroprotective effects and relates to the repair of the CNS [14]. Furthermore, G93A SOD1 and MT-3 double KO mice exhibited earlier progression of amyotrophic lateral sclerosis (ALS) [16]. These findings indicate that MT-3 has neuroprotective effects in acute and chronic phases of diseases. Moreover, Rahman et al. reported the hair concentrations of Zn and Ca decreased and the concentrations of Cu and Cd increased in schizophrenic patients [18]. So the alteration in the metabolism of heavy metals is suspected as a risk factor of schizophrenia. On the other hand, there were no reports about the relationship between psychological disorders and MT-3.

In general, less social interaction is observed in schizophrenia, anxiety, autism, and phencyclidine-induced psychosis [15]. Especially, autism is a brain development disorder characterized by impaired social interaction and communication. The plasma zinc/serum copper ratio plays a role in causing autism [6]. Moreover, MTs attenuate the neurotoxicity of mercury which plays an etiologic role in autism [1]. In addition, lower PPI is observed in schizophrenia and autism [7]. In particular, PPI abnormality is observed in both human patients and animal models of schizophrenia; thus, it is well studied and reliable for investigation of schizophrenia [2]. Acoustic prepulses for PPI are regulated by forebrain circuits including the inferior colliculus, mesolimbic cortex, nucleus accumbens, ventral pallidum, thalamus, and pedunculopontine tegmentum nucleus [7]. In general, PPI deficit and negative symptom of schizophrenia are related to the prefrontal dysfunction. Taken together, MT-3 may correlate to neuron development in these lesions. However, there were no significant differences between MT-3 KO and WT mice in total dendritic length, number of branches, and spine density in pyramidal neurons in layers II/III and V of the prefrontal cortex (PFC) (data not shown). To clarify the detailed mechanisms of PPI abnormalities, molecular biological studies will be needed.

To examine psychological disorders such as schizophrenia and autism, many animal models were found and used. Animal models exhibited various symptoms and defects upon examination. However, some animals exhibit too many symptoms; thus sometimes causing the researchers to be confused and distressed. While MT-3 KO mice were impaired in social interaction and PPI, their spontaneous locomotor activity, habituation, learning and memory were normal. MT-3 KO mice also have normal life spans and reproductive potential. Taken together, they may be suitable subjects to investigate psychological disorders. Further experiments will be needed to clarify the relationship between MT-3 and psychological diseases.

References

[1] M. Aschner, T. Syversen, D.O. Souza, J.B. Rocha, Metallothioneins: mercury species-specific induction and their potential role in attenuating neurotoxicity, Exp. Biol. Med. (Maywood) 231 (2006) 1468–1473.
[2] D.L Braff, M.A. Geyer, Sensorimotor gating and schizophrenia. Human and animal model studies, Arch. Gen. Psychiatry 47 (1990) 181–188.
[3] Z.C Ding, Q. Zheng, B. Cai, F.Y. Ni, W.H. Yu, X.C. Teng, Y. Gao, F. Liu, D. Chen, Y. Wang, H.M. Wu, H.Z. Sun, M.J. Zhang, X.S. Tan, Z.X. Huang, Study on structure-property-reactivity-function relationship of human neuronal growth inhibitory factor (hGIF), J. Inorg. Biochem. 102 (2008) 1965–1972.
[4] J.C. Erickson, G. Hollopeter, S.A. Thomas, G.J. Froelick, R.D. Palmiter, Disruption of the metallothionein-III gene in mice: analysis of brain zinc, behavior,

and neuron vulnerability to metals, aging, and seizures, J. Neurosci. 17 (1997) 1271–1281.
[5] J.C. Erickson, A.K. Sewell, L.T. Jensen, D.R. Winge, R.D. Palmiter, Enhanced neurotrophic activity in Alzheimer's disease cortex is not associated with down-regulation of metallothionein-III (GIF), Brain Res. 649 (1994) 297–304.
[6] S. Faber, G.M. Zinn, J.C. Kern 2nd, H.M. Kingston, The plasma zinc/serum copper ratio as a biomarker in children with autism spectrum disorders, Biomarkers 14 (2009) 171–180.
[7] M. Fendt, L. Li, J.S. Yeomans, Brain stem circuits mediating prepulse inhibition of the startle reflex, Psychopharmacology (Berl) 156 (2001) 216–224.
[8] S.E File, The use of social interaction as a method for detecting anxiolytic activity of chlordiazepoxide-like drugs, J. Neurosci. Methods 2 (1980) 219–238.
[9] M.A Geyer, N.R. Swerdlow, R.S. Mansbach, D.L. Braff, Startle response models of sensorimotor gating and habituation deficits in schizophrenia, Brain Res. Bull. 25 (1990) 485–498.
[10] J. Hidalgo, M. Aschner, P. Zatta, M. Vasák, Roles of the metallothionein family of proteins in the central nervous system, Brain Res. Bull. 55 (2001) 133–145.
[11] I. Hozumi, T. Inuzuka, M. Hiraiwa, Y. Uchida, T. Anezaki, H. Ishiguro, H. Kobayashi, Y. Uda, T. Miyatake, S. Tsuji, Changes of growth inhibitory factor after stab wounds in rat brain, Brain Res. 688 (1995) 143–148.
[12] I. Hozumi, T. Inuzuka, S. Tsuji, Brain injury and growth inhibitory factor (GIF)—a mini review, Neurochem. Res. 23 (1998) 319–328.
[13] I. Hozumi, Y. Uchida, K. Watabe, T. Sakamoto, T. Inuzuka, Growth inhibitory factor (GIF) can protect from brain damage due to stab wounds in rat brain, Neurosci. Lett. 395 (2006) 220–223.
[14] T. Inuzuka, I. Hozumi, A. Tamura, M. Hiraiwa, S. Tsuji, Patterns of growth inhibitory factor (GIF) and glial fibrillary acidic protein relative level changes differ following left middle cerebral artery occlusion in rats, Brain Res. 709 (1996) 151–231.
[15] T.A Jenkins, M.K. Harte, C.E. McKibben, J.J. Elliott, G.P. Reynolds, Disturbances in social interaction occur along with pathophysiological deficits following subchronic phencyclidine administration in the rat, Behav. Brain Res. 194 (2008) 230–235.
[16] K. Puttaparthi, W.L. Gitomer, U. Krishnan, M. Son, B. Rajendran, J.L. Elliott, Disease progression in a transgenic model of familial amyotrophic lateral sclerosis is dependent on both neuronal and non-neuronal zinc binding proteins, J. Neurosci. 22 (2002) 8790–8796.
[17] H. Qiao, Y. Noda, H. Kamei, T. Nagai, H. Furukawa, H. Miura, Y. Kayukawa, T. Ohta, T. Nabeshima, Clozapine, but not haloperidol, reverses social behavior deficit in mice during withdrawal from chronic phencyclidine treatment? Neuroreport 12 (2001) 11–15.
[18] A. Rahman, M.A. Azad, I. Hossain, M.M. Qusar, W. Bari, F. Begum, S.M. Huq, A. Hasnat, Zinc, manganese, calcium, copper, and cadmium level in scalp hair samples of schizophrenic patients, Biol. Trace Elem. Res. 127 (2009) 102–108.
[19] N.R. Swerdlow, M.A. Geyer, Using an animal model of deficient sensorimotor gating to study the pathophysiology and new treatments of schizophrenia, Schizophr. Bull. 24 (1998) 285–301.
[20] N. Thirumoorthy, K.T. Manisenthil Kumar, A. Shyam Sundar, L. Panayappan, M. Chatterjee, Metallothionein: an overview, World J. Gastroenterol. 13 (2007) 993–996.
[21] A.K. West, J. Hidalgo, D. Eddins, E.D. Levin, M. Aschner, Metallothionein in the central nervous system: roles in protection, regeneration and cognition, Neurotoxicology 29 (2008) 489–503.
[22] S Yanagitani, H. Miyazaki, Y. Nakahashi, K. Kuno, Y. Ueno, M. Matsushita, Y. Naitoh, S. Taketani, K. Inoue, Ischemia induces metallothionein III expression in neurons of rat brain, Life Sci. 64 (1999) 707–715.

Neurobiology of Disease 36 (2009) 470–476

Contents lists available at ScienceDirect

Neurobiology of Disease

journal homepage: www.elsevier.com/locate/ynbdi

Involvement of CHOP, an ER-stress apoptotic mediator, in both human sporadic ALS and ALS model mice

Yasushi Ito [a], Mitsunori Yamada [b,c], Hirotaka Tanaka [a], Kazunari Aida [a], Kazuhiro Tsuruma [a], Masamitsu Shimazawa [a], Isao Hozumi [d], Takashi Inuzuka [d], Hitoshi Takahashi [c], Hideaki Hara [a,*]

[a] Department of Biofunctional Evaluation, Molecular Pharmacology, Gifu Pharmaceutical University, 5-6-1 Mitahora-higashi, Gifu 502-8585, Japan
[b] Department of Clinical Research, National Hospital Organization, Saigata National Hospital, 468-1 Saigata, Ohgata-ku Johetsu-city, Niigata 949-3193, Japan
[c] Department of Pathology, Brain Research Institute, Niigata University, 1-757, Asahimachi-dori, Chuo-ku, Niigata 951-8585, Japan
[d] Department of Neurology and Geriatrics, Gifu University Graduate School of Medicine, 1-1, Yanagido, Gifu 501-1194, Japan

ARTICLE INFO

Article history:
Received 16 June 2009
Revised 17 August 2009
Accepted 28 August 2009
Available online 4 September 2009

Keywords:
Amyotrophic lateral sclerosis (ALS)
Astrocyte
C/EBP homologous protein (CHOP)
Endoplasmic reticulum (ER) stress
Superoxide dismutase 1 (SOD1)
Spinal cord

ABSTRACT

Endoplasmic reticulum (ER) stress-induced neuronal death may play a critical role in the pathogenesis of amyotrophic lateral sclerosis (ALS). However, whether CCAAT/enhancer binding protein (C/EBP) homologous protein (CHOP), an ER-stress apoptotic mediator, is involved in the pathogenesis of ALS is controversial. Here we demonstrate the expression levels and localization of CHOP in spinal cords of both sporadic ALS patients and ALS transgenic mice by immunohistochemistry. In the spinal cords of sporadic ALS patients, CHOP was markedly up-regulated but typically expressed at low levels in those of the control. Likewise, CHOP expression increased at 14 (symptomatic stage) and 18 to 20 weeks (end stage) in ALS transgenic mice spinal cords. Furthermore, localizations of CHOP were merged in motor neurons and glial cells, such as oligodendrocytes, astrocytes, and microglia. These results indicate that the up-regulation of CHOP in motor neurons and glial cells may play pivotal roles in the pathogenesis of ALS.

Introduction

Amyotrophic lateral sclerosis (ALS) is a progressive fatal neurodegenerative disease characterized by the death of motor neurons in the spinal cord, motor cortex, and brain stem, leading to muscle atrophy and paralysis (Cleveland and Rothstein, 2001). The majority of ALS cases are considered sporadic. Approximately 5–10% of cases are familial ALS, and of these, 20–25% are caused by mutations in the gene encoding Cu/Zn superoxide dismutase 1 (SOD1), an enzyme that catalyzes the dismutation of superoxide into oxygen and hydrogen peroxide (Rosen et al., 1993). Transgenic rodents overexpressing human mutant SOD1 (mSOD1) develop an ALS-like phenotype of progressive motor neuron degeneration with a reduced lifespan (Gurney et al., 1994; Nagai et al., 2001).

Although the precise etiology of ALS remains unclear, recent studies of autopsied tissue samples of sporadic ALS patients and *in vivo* experiments with tissue from $SOD1^{G93A}$ rodents indicate that endoplasmic reticulum (ER) stress is involved in the pathogenesis of ALS (Kikuchi et al., 2006; Ilieva et al., 2007; Atkin et al., 2008). ER stress is triggered when misfolded or unfolded proteins accumulate in the lumen, leading to the ER stress response known as unfold protein response (UPR) (Harding et al., 2002; Rutkowski and Kaufman, 2004). Although UPR improves the ability of protein folding by inducing ER resident chaperones and protects the cell from ER stress (Harding et al., 2002; Rutkowski and Kaufman, 2004), the excessive ER stress leads to apoptosis (Breckenridge et al., 2003; Oyadomari and Mori, 2004; Rao et al., 2004). One of the components of the ER stress-mediated apoptosis pathway is C/EBP homologous protein (CHOP, also known as GADD153), which is a transcription factor activated during ER stress (Oyadomari and Mori, 2004). Recent studies have suggested that ER stress signaling is involved in the motor neuron death in ALS (Tobisawa et al., 2003; Kikuchi et al., 2006; Atkin et al., 2008). However, whether CHOP is involved in the pathogenesis of ALS is controversial because expression of CHOP has been reported both as unchanged (Wootz et al., 2004) or up-regulated at disease onset (Vlug et al., 2005; Atkin et al., 2008) in patients with sporadic ALS and $SOD1^{G93A}$ mouse spinal cords according to immunoblotting. Furthermore, it has not been clear where CHOP expressions increase in ALS spinal cord because protein extraction methods for immunoblot analysis in previous reports were not focused on spinal cord level. Therefore, it is important to study CHOP expressions in multiple levels of spinal cord in sporadic ALS and $SOD1^{G93A}$ mouse tissue. We therefore investigated the expression level and localization of CHOP using an immunohistological technique in the tissue of patients with sporadic ALS and $SOD1^{G93A}$ mouse spinal cords.

* Corresponding author. Fax: +81 58 237 8596.
E-mail address: hidehara@gifu-pu.ac.jp (H. Hara).
Available online on ScienceDirect (www.sciencedirect.com).

0969-9961/$ - see front matter © 2009 Elsevier Inc. All rights reserved.
doi:10.1016/j.nbd.2009.08.013

Materials and methods

Tissue sample

Human spinal cord

Spinal cord segments were taken at autopsy from ten patients with features typical of sporadic ALS. Spinal cord tissue from 11 individuals without history/evidence of neurological or psychiatric disease was taken for the control samples (Table 1). Three paraffin-embedded coronal sections cut at 4-μm thickness through the spinal cord [cervical spinal cord (C7), thoracic spinal cord (T8), and lumbar spinal cord (L4)] were prepared in the standard manner.

Mice spinal cord

Transgenic mice expressing a G93A mutant of human SOD1 [strain B6SJL-TgN (SOD1-G93A)1Gur] ($SOD1^{G93A}$) were obtained from the Jackson Laboratory (Bar Harbor, ME, USA). Three groups of $SOD1^{G93A}$ mice at 10 (asymptomatic-stage), 14 (symptomatic-stage), and 18 to 20 weeks (end-stage) and their age- and gender-matched wild-type (WT) littermates were used. At the end of their assigned survival periods, the mice were anesthetized with sodium pentobarbital (80 mg/kg, i.p.) (Nembutal, Dainippon, Osaka, Japan), and perfused with 2% (w/v) paraformaldehyde solution in 0.01 M PBS. The spinal cords were removed after 15-min perfusion at 4 °C, immersed in the same fixative solution for 24 h, soaked in 25% (w/v) sucrose for 1 day, and then frozen in embedding compound (Tissue-Tek, Sakura Finetechnical Co. Ltd., Tokyo, Japan). Every sixth section at 1-mm intervals was cut at 20-μm thickness and mounted onto a glass slide (L1-1, L1-2, L2-1, L2-2, L3-1, and L3-2). All experiments were approved and monitored by the Institutional Animal Care and Use Committee of Gifu Pharmaceutical University.

Immunohistochemistry

For immunohistochemistry, coronal sections of spinal cord were placed on slides (MASCOAT; Matsunami, Osaka, Japan), washed with 0.01 M PBS, and then treated with 0.3% hydrogen peroxidase in 0.01 M PBS for 30 min at room temperature. Next, the sections were preincubated with 10% normal goat serum (Vector) in 0.01 M PBS for 30 min and then incubated for 1 day at 4 °C with specific rabbit anti-CHOP polyclonal antibody (F-168; 1:1000, Santa Cruz Biotechnology, CA, USA) in the following solution: 10% normal goat serum in 0.01 M PBS containing 0.3% (v/v) Triton X-100. They were washed with 0.01 M PBS and then incubated with biotinylated anti-rabbit IgG before being incubated with the avidin–biotin–peroxidase complex for 30 min at room temperature, and finally visualized using DAB as a peroxidase substrate.

To visualize co-localization of CHOP with (i) neurofilament H non-phosphorylated (SMI 32) or choline acetyltransferase (ChAT), (ii) adenomatous polyposis coli (APC), (iii) glial fibrillary acidic protein (GFAP), or (iv) cluster of differentiation antigen-11b (CD11b) double immunofluorescence was performed on spinal cord sections from humans and mice. Coronal sections of the spinal cords were washed with 0.01 M PBS, preincubated with 10% normal goat serum in 0.01 M PBS for 30 min, and then incubated overnight at 4 °C with rabbit anti-CHOP polyclonal antibody (1: 1000 dilution) in the following solution: 10% normal goat serum in 0.01 M PBS with 0.3% (v/v) Triton X-100. Sections were blocked with M.O.M. blocking reagent (M. O.M. immunodetection kit; Vector) and then incubated either with mouse anti-SMI32 monoclonal antibody (NE1023; 1:1000, Calbiochem, San Diego, CA, USA), mouse anti-APC monoclonal antibody (1:250), mouse anti-GFAP monoclonal antibody (1:600), or mouse anti-CD11b (1:1000) monoclonal anti-body for 1 day at 4 °C. They were washed with 0.01 M PBS and then incubated for 3 h at room temperature with a mixture of Alexa Fluor 488 $F(ab')_2$ fragment of goat anti-rabbit IgG (H+L) (1:1000 dilution) (Molecular Probes, Eugene, OR) and Alexa Fluor 546 $F(ab')_2$ fragment of goat anti-mouse IgG (H+L) (1:1000 dilution) (Molecular Probes).

In the immunostaining procedures for CHOP with ChAT, coronal sections of the spinal cords were washed with 0.01 M PBS, preincubated with 10% normal goat serum in 0.01 M PBS for 30 min, and then incubated overnight at 4 °C with rabbit anti-CHOP

Table 1
Clinical information about the spinal cord tissues from patients with sporadic ALS (a), and for control (b).

(a) Sporadic ALS

Case	Age of death (years)	Sex	PMI (h)	Disease duration (months)
1	59	M	3.2	48
2	83	F	2.3	8
3	57	M	2.5	9
4	76	M	1.7	22
5	74	M	5.0	12
6	64	M	1.5	18
7	80	M	2.7	72
8	78	F	1.8	18
9	49	F	2.5	40
10	73	M	[a]	48
Mean ± S.E.M.	69.3 ± 3.6		2.6 ± 0.4	29.5 ± 6.8

(b) Control

Case	Age of death (years)	Sex	PMI (h)	Cause of death
1	68	M	3.8	Myopathy
2	73	M	3.3	Multiple cerebral infarction
3	80	M	3.0	Hemoperitoneum
4	64	F	2.0	Polymyositis
5	73	M	3.3	Multiple cerebral infarction
6	70	F	3.8	brainstem infarction
7	62	M	3.4	basilar artery aneurysm
8	71	F	[a]	Myoclonus epilepsy
9	70	M	2.0	Multiple cerebral infarction
10	82	M	6.0	Multiple cerebral infarction
11	76	M	3.4	Multiple cerebral infarction
Mean ± S.E.M.	71.3 ± 1.8		3.4 ± 0.4	

M, male; F, female; PMI, post mortem interval.
[a] The exact time was not known.

polyclonal antibody (1: 1000 dilution) in the following solution: 10% normal goat serum in 0.01 M PBS with 0.3% (v/v) Triton X-100. Sections were washed with 0.01 M PBS, preincubated with 10% normal rabbit serum in 0.01 M PBS for 30 min, and then incubated overnight at 4 °C with goat anti-ChAT polyclonal antibody (1: 5000 dilution) in the following solution: 10% normal rabbit serum in 0.01 M PBS with 0.3% (v/v) Triton X-100. They were washed with 0.01 M PBS and then incubated for 3 h at room temperature with a mixture of Alexa Fluor 488 $F(ab')_2$ fragment of goat anti-rabbit IgG (H+L) (1:1000 dilution) (Molecular Probes, Eugene, OR) and Alexa Fluor 546 $F(ab')_2$ fragment of rabbit anti-goat IgG (H+L) (1:1000 dilution) (Molecular Probes).

Cell count

To assess the number of CHOP-positive cells in the Rexed laminae IX anterior horn (AH) in the human spinal cord, sections immunostained with CHOP were used for cell counting: C7, T8, and L4 in the spinal cords of the control patients and patients with sporadic ALS, respectively (Fig. 1). In the Rexed laminae IX AH in the lumbar spinal cords of the mice, sections immunostained with CHOP were used for cell counting: six equally spaced sections (interval, 1 mm) from L1 to L3 for the lumbar spinal cord (L1-1, L1-2, L2-1, L2-2, L3-1, and L3-2) in each mouse (Fig. 2). The area used for cell counting was 0.036 mm^2 of each side in the spinal cord. Cell counts were carried out under a microscope at 400× magnification in a masked fashion by a single observer (Y.I.). Total cell numbers were calculated from six sections in each group. Care was taken to count only clearly visible cells in this condition.

Statistical analysis

Data are presented as means ± S.E.M. Statistical comparisons (one-way ANOVA followed by a Dunnett's test) were made using STAT VIEW version 5.0 (SAS Institute, Inc., Cary, NC, USA). A value of $P<0.05$ was considered to indicate statistical significance.

Results

The number of CHOP-positive cells in spinal cord

Representative photographs are shown for the spinal cord tissue of the control patients and patients with sporadic ALS immunostained with CHOP [C7 (Fig. 1A, a) and (Fig. 1B, b), T8 (Fig. 1C, c) and (Fig. 1D, d), and L4 (Fig. 1E, e) and (Fig. 1F, f), respectively]. In the spinal cords of the patients with sporadic ALS, the expression level of CHOP was markedly up-regulated, but typically expressed at low levels in that of the spinal cords of the control patients in any sections C7, T8, and L4, respectively. The number of CHOP-positive cells in the Rexed laminae IX AH in the spinal cords of the patients with sporadic ALS (4.6 ± 0.4, 4.4 ± 0.7, and 3.4 ± 0.6 in sections C7, T8, and L4, respectively, $n=10$) was significantly larger than in the control patients (0.9 ± 0.3, 1.2 ± 0.3, and 1.0 ± 0.2 in sections C7, T8, and L4, respectively, $n=11$; $P<0.01$ in each case) (Fig. 1M).

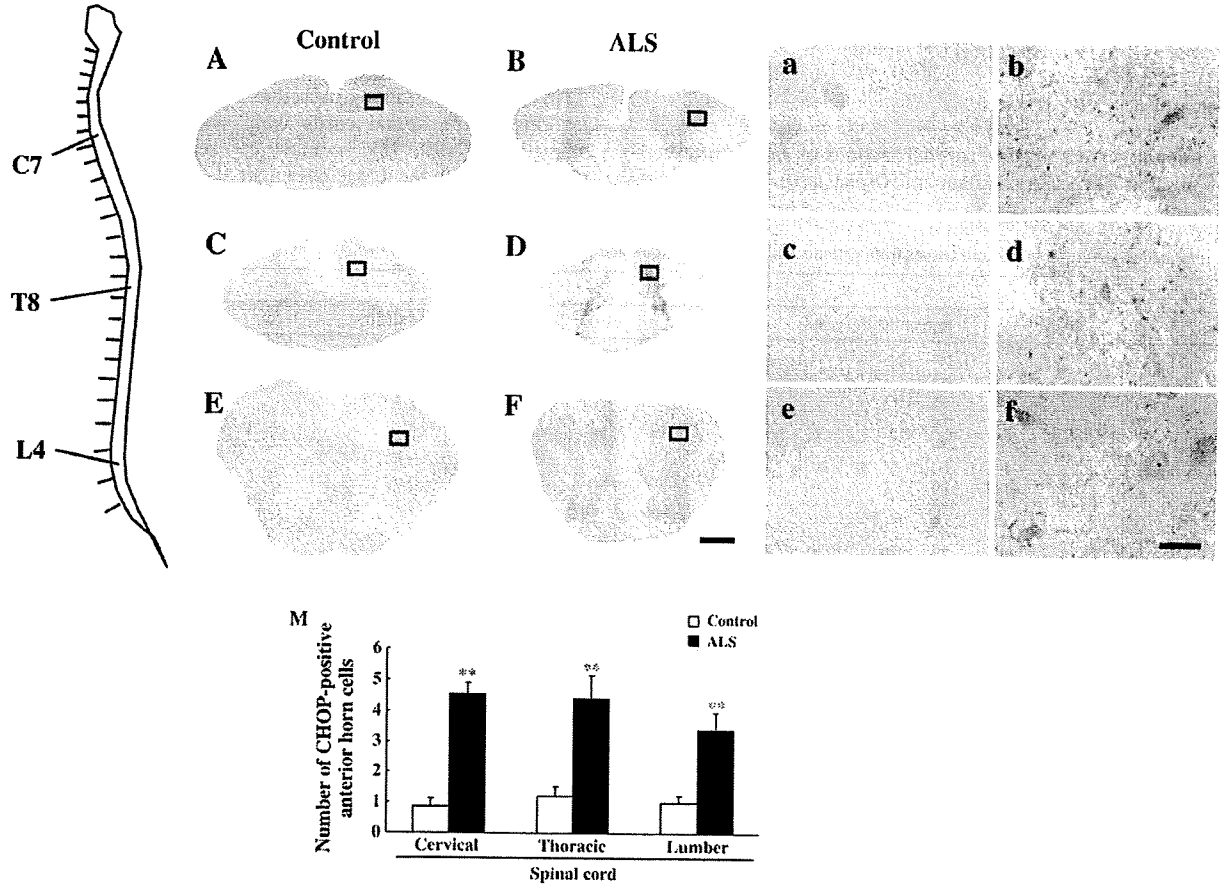

Fig. 1. Human spinal cord tissue section. Representative photographs are shown for control patients and patients sporadic ALS, C: cervical spinal cord (A, a) and (B, b), T: thoracic spinal cord (C, c) and (D, d), and L: lumbar spinal cord (E, e) and (F, f), respectively. Scale bars = 1 mm (A, B, C, D, E, and F), and 65 μm (a, b, c, d, e, and f). Average number of CHOP-positive anterior horn cells in the human spinal cord (M). Each value represents the mean ± S.E.M. for 10 or 11 spinal cords. *$P<0.05$, **$P<0.01$ vs. control (Dunnett's test).

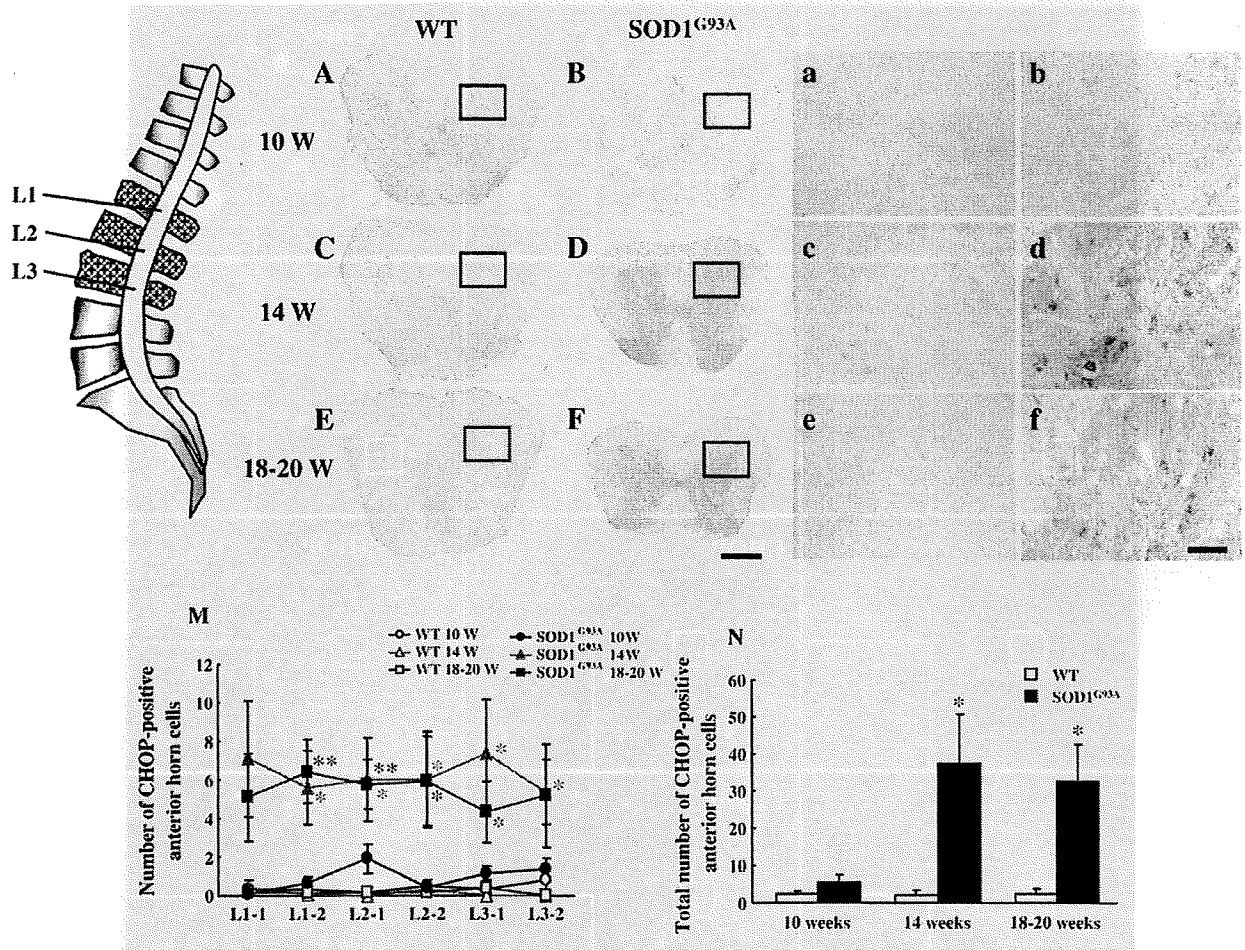

Fig. 2. Spinal cord tissue section of SOD1^{G93A} mice. Representative photographs are shown for wild-type mice at 10 (A, a), 14 (C, c), and 18 to 20 weeks (E, e) and for SOD1^{G93A} mice at 10 (B, b), 14 (D, d), and 18 to 20 weeks (F, f). Scale bar = 350 μm (A, B, C, D, E, and F), and 65 μm (a, b, c, d, e, and f). Average number of CHOP-positive anterior horn cells in mice (per 0.036 mm^2 tissue area) (M). Total number of CHOP-positive anterior horn cells obtained from 6 sections (L1-1, L1-2, L2-1, L2-2, L3-1, and L3-2) (N). Each value represents the mean ± S.E.M. for 6 spinal cords. *P<0.05, **P<0.01 vs. wild-type (Dunnett's test).

Furthermore, representative photographs are shown for the WT mice at 10 (Fig. 2A, a), 14 (Fig. 2C, c), and 18 to 20 weeks (Fig. 2E, e) and for SOD1^{G93A} mice at 10 (Fig. 2B, b), 14 (Fig. 2D, d), and 18 to 20 weeks (Fig. 2F, f) in spinal cord tissue. In the SOD1^{G93A} mice spinal cord, the expression level of CHOP was markedly up-regulated, but typically expressed at low levels in that of the WT mice at 14 and 18 to 20 weeks, respectively. In the Rexed laminae IX AH of the lumbar spinal cords of the mice, CHOP-positive cell counts obtained for the SOD1^{G93A} mice at 14 weeks were 7.1 ± 3.0, 5.6 ± 1.9, 6.0 ± 2.2, 6.0 ± 2.5, 7.3 ± 2.8, and 5.3 ± 1.7 in sections L1-1, L1-2, L2-1, L2-2, L3-1, and L3-2, respectively (each n = 6). Each of these counts was greater than the corresponding one for the WT mice at 14 weeks (0.4 ± 0.4, 0.1 ± 0.1, 0 ± 0, 0.3 ± 0.3, 0 ± 0, and 0 ± 0, respectively, each n = 6; P<0.05 in each case). The SOD1^{G93A} mice at 18 to 20 weeks (5.1 ± 2.3, 6.4 ± 1.6, 5.8 ± 1.3, 5.9 ± 2.4, 4.3 ± 1.6, and 5.2 ± 2.7 in sections L1-1, L1-2, L2-1, L2-2, L3-1, and L3-2, respectively, each n = 6) also exhibited significantly greater CHOP-positive cell numbers in the AH in the lumbar spinal cord than the WT mice at 18 to 20 weeks (0.2 ± 0.2, 0.2 ± 0.2, 0.2 ± 0.2, 0.2 ± 0.2, 0.4 ± 0.4, and 0 ± 0, respectively, each n = 6; P<0.05 in each case) (Fig. 2M). Likewise, the total CHOP-positive cell numbers in the AH in the lumbar spinal cord (L1 to L3) for the SOD1^{G93A} mice at 14 and 18 to 20 weeks were significantly greater (37.3 ± 13.4 and 32.7 ± 10.1, respectively, n = 6) than that for the WT mice at 14 and 18 to 20 weeks (2.0 ± 1.3 and 2.3 ± 1.2, respectively, n = 6) (Fig. 2N). In contrast, there were no significant differences in numbers of CHOP-positive cell between the SOD1^{G93A} mice at 10 weeks and the WT mice at 10 weeks (Fig. 2N).

Double immunofluorescence

To identify CHOP-positive cells, double immunofluorescence was performed for CHOP and SMI 32, APC, GFAP, or CD11b in the Rexed laminae IX AH in the spinal cords of patients with sporadic ALS, respectively. SMI 32-positive motor neurons were found to express CHOP in the Rexed laminae IX AH in the spinal cords of patients with sporadic ALS (Fig. 3). Furthermore, APC-positive oligodendrocytes, GFAP-positive astrocytes, and CD11b-positive microglia were also immunoreactive for CHOP (Fig. 3).

Likewise, to identify CHOP-positive cells in the Rexed laminae IX AH in the mice spinal cord, double immunofluorescence was performed for CHOP and ChAT, APC, GFAP, or CD11b, respectively. In SOD1^{G93A} mice at 14 and 18 to 20 weeks, ChAT-positive motor neurons, APC-positive oligodendrocytes, GFAP-positive astrocytes, and CD11b-positive microglia also expressed CHOP (Fig. 4).

Discussion

In this study, we investigated the expression level and localization of CHOP by immunostaining in spinal cord tissue from patients with sporadic ALS and SOD1^{G93A} mice. We provided evidence of increased

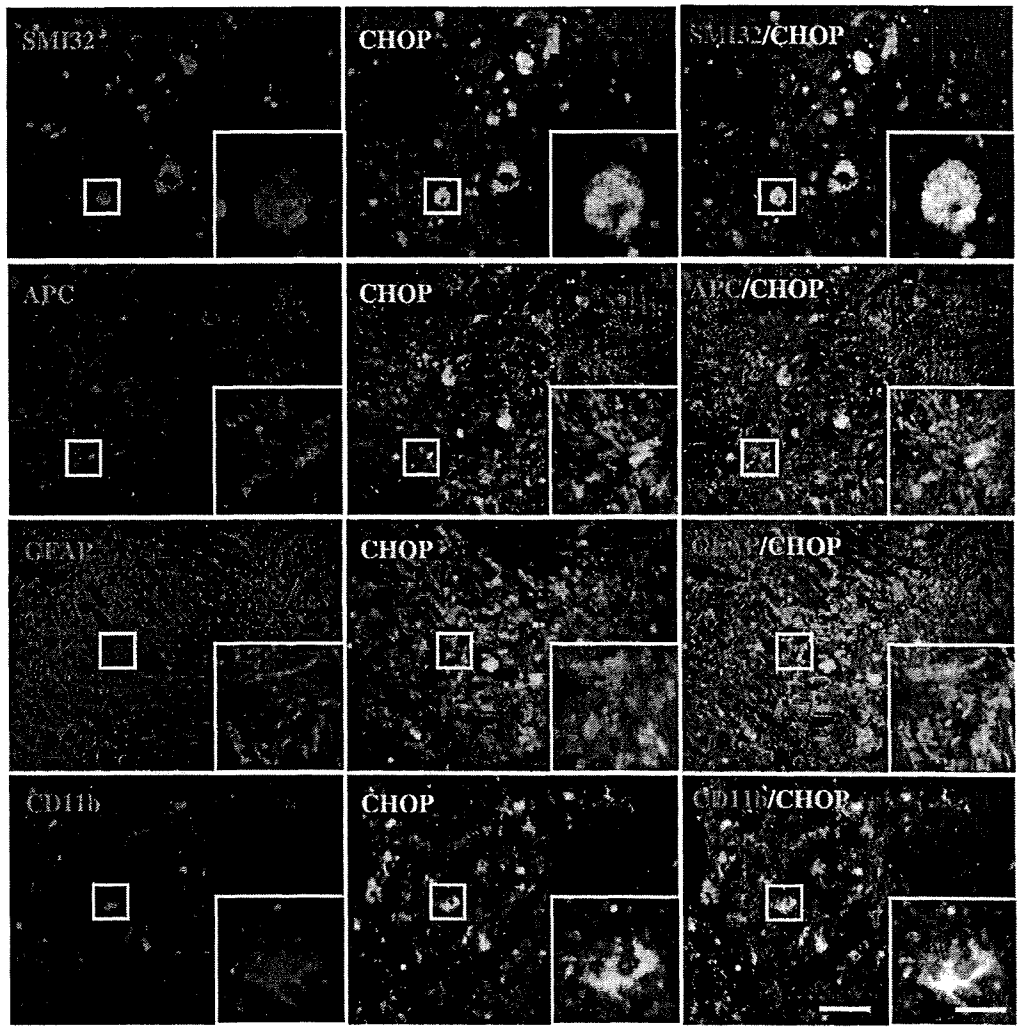

Fig. 3. Immunolocalization of CHOP in the spinal cords of patients with sporadic ALS. Representative photographs showing SMI32/CHOP, APC/CHOP, GFAP/CHOP, and CD11b/CHOP double-immunostaining in the anterior horn of the spinal cords of patients with sporadic ALS. Scale bar = 40 μm. Boxed areas are shown at higher magnification. Scale bar = 10 μm.

expression of CHOP and colocalization with motor neurons, oligodendrocytes, astrocytes, and microglia in the AH of the spinal cords of both patients with sporadic ALS and SOD1^{G93A} mice.

In the present study, the number of CHOP-positive cells in the AH of the spinal cords of patients with sporadic ALS was significantly greater than that of the control tissue. Previous studies have shown that the first stages of UPR, including the expressions of stress sensor kinases inositol requiring enzyme 1 (IRE1), double-stranded RNA-dependent protein kinase (PKR)-like ER kinase (PERK), and activating transcription factor-6 (ATF-6), and protein disulfide isomerase (PDI) family members were already underway in the spinal cords of patients with sporadic ALS, in addition to CHOP by Western blotting (Ilieva et al., 2007; Atkin et al., 2008). Combined with these reports, our findings suggest that ER stress, especially CHOP, was involved in the pathogenesis of sporadic ALS.

In SOD1^{G93A} mice, the level of CHOP expression also increased at 14 (symptomatic stage) and 18 to 20 weeks (end stage), but not 10 weeks (asymptomatic stage) in the AH of the spinal cords in the present study. This might provide an answer why the major symptoms of ALS patients with mSOD1-linked familial ALS do not develop until specific times late in life (age-related onset), even though the mutant proteins are expressed throughout life. A recent study also suggested that age-related changes occurred in response to ER stress in SOD1^{G93A} mice (Saxena et al., 2009). In general, newly synthesized and misfolded proteins are refolded by chaperons such as regulated protein 78 (GRP78), regulated protein 94 (GRP94), PDI, calnexin, and calreticulin (Jørgensen et al., 2003; Szegezdi et al., 2006; Wei et al., 2008). These UPR may be more robust in younger familial ALS patients and might be the reason that protein aggregations are not observed in young patients even though mSOD1 is expressed. However, age-related decreases in protein folding or chaperone capability may occur, and accumulation of misfolded proteins in the ER lumen may gradually lead to ER stress (Bassik et al., 2004; Lindholm et al., 2006; Turner and Atkin, 2006). In fact, the ER pathological hallmarks of ALS show the possible involvement of ER stress associated with impaired protein production (Oyanagi et al., 2008; Kanekura et al., 2009). Previous reports suggested that mSOD1 retention in the ER in COS7 cells (Tobisawa et al., 2003) and age-related increase of mSOD1 aggregation to ER in the spinal cords of SOD1^{G93A} mice (Kikuchi et al., 2006). Prolonged ER stress associated with insufficient degradation of misfolded proteins would subsequently activate apoptotic pathways (Sekine et al., 2006; Turner et al., 2006). However, it is not clear whether CHOP is involved in the pathogenesis of SOD1^{G93A} mice. Some investigators reported that expression of CHOP remained unchanged (Wootz et al., 2004; Nagata et al., 2007), while others reported that CHOP was up-regulated at disease onset in SOD1^{G93A} mice spinal cords (Vlug et al., 2005; Atkin et al., 2006; Kieran et al., 2007). These findings indicated CHOP may

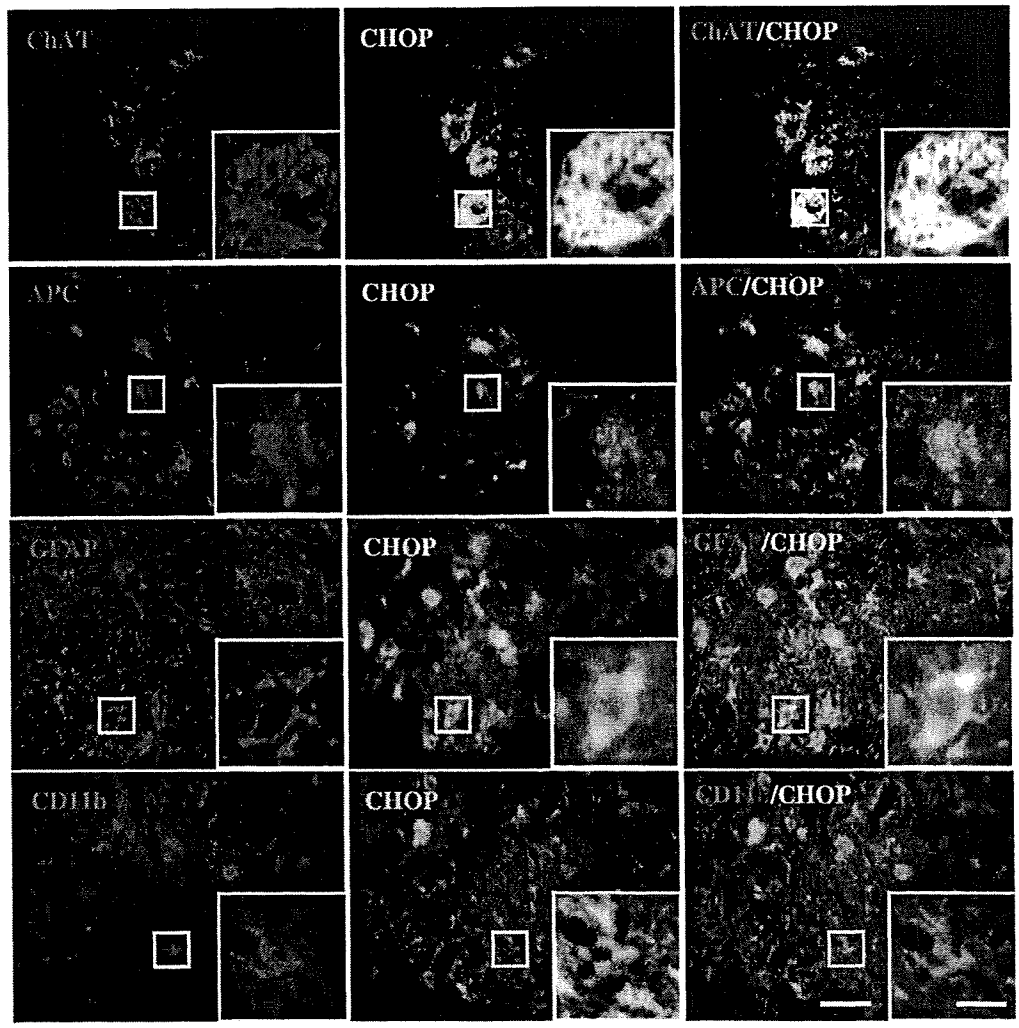

Fig. 4. Immunolocalization of CHOP in SOD1^{G93A} mice spinal cord. Representative photographs showing ChAT/CHOP and APC/CHOP double-immunostaining in the anterior horn of SOD1^{G93A} mice spinal cord at 14 weeks (symptomatic-stage). Representative photographs showing GFAP/CHOP and CD11b/CHOP double-immunostaining in the anterior horn of the SOD1^{G93A} mice spinal cord at 18 to 20 weeks (end-stage). Scale bar = 40 μm. Boxed areas are shown at higher magnification. Scale bar = 10 μm.

increase only transiently in SOD1^{G93A} mice spinal cords. Therefore, in the present study, the up-regulation of CHOP may be observed from symptom- (14 weeks) to end-stage (18 to 20 weeks). Taken together with previous studies and our findings, the time-dependent (age-related) increase of CHOP may be involved in the motor neuron death in SOD1^{G93A} mice spinal cords.

Here, we provide evidence for up-regulation of CHOP in the AH of the spinal cords of both patients with sporadic ALS and SOD1^{G93A} mice. Next, we investigated where CHOP is expressed. In the present study, localizations of CHOP were not only in motor neurons but also in glial cells, such as oligodendrocytes, astrocytes, and microglia. However, the mechanisms by which CHOP induces apoptosis in different systems remain uncertain (Matsumoto et al., 1996; Eymin et al., 1997; Fontanier-Razzaq et al., 1999; Maytin et al., 2001). Regarding the intracellular localization of CHOP, it is well known that its low expression in the cytoplasm under normal conditions is robustly increased by ER stress, and then accumulates in the nucleus (Ron and Habener, 1992). In the present study, we showed CHOP upregulation in the nucleus, and some cells in the cytoplasm. In these cells that expressing CHOP in the cytoplasm, CHOP translocation to the nucleus may appear to be in a later phase. We found the presence of CHOP in motor neurons and oligodendrocytes whose apoptotic program is activated in the AH of the spinal cords of both patients with sporadic ALS and SOD1^{G93A} mice. In fact, we observed a significant loss of motor neurons in the AH of the spinal cords of SOD1^{G93A} mice at 14 and 18 to 20 weeks (data not shown).

However, the disease onset of ALS is non-cell autonomous, and mSOD1 damage within cell types other than motor neurons and oligodendrocytes may be a central contributor to the initiation of motor neuron degeneration (Yamanaka et al., 2008). Another new finding of the present study is the observation that astrocytes express CHOP in the AH in the spinal cords of both patients with sporadic ALS and SOD1^{G93A} mice. Although the expression of mutated human SOD1 in primary mouse spinal motor neurons does not provoke motor neuron degeneration, rodent astrocytes expressing mSOD1 kill spinal primary and embryonic mouse stem cell-derived motor neurons (Nagai et al., 2007). In fact, GFAP-positive astrocytes significantly increased time-dependently in the AH of the spinal cords of SOD1^{G93A} mice at 14 and 18 to 20 weeks (data not shown). In addition, although GFAP-positive astrocytes express high CHOP levels after spinal cord injury in rats, astrocytes are able to survive (Park et al., 2004; Penas et al., 2007). Therefore, CHOP-positive astrocytes may play a role in the specific degeneration of spinal motor neurons in ALS.

Recently, it has been reported that diminishing mSOD1 toxicity within microglia significantly slowed disease progression of ALS (Yamanaka and Yamashita, 2007). The diminished toxicity had little

effect on the early disease phase, but sharply slowed later disease progression (Boillée et al., 2006). Consistent with these findings, CD11b-positive microglia increased slightly in the early disease phase (until 10 weeks), but increased sharply in later disease progression (14–20 weeks) in the AH of the spinal cords of $SOD1^{G93A}$ mice (data not shown). In addition, a previous study suggested that nitric oxide, an important contributor to neuronal damage, induced apoptosis in microglia, which occurs through the ER stress pathway involving CHOP (Kawahara et al., 2004), indicating the active role of microglia in the disease progression of ALS.

In conclusion, these findings indicate that CHOP, one of the components of the ER stress-mediated apoptosis pathway, may be involved in the pathogenesis of ALS, and the up-regulation of CHOP protein levels in motor neurons and glial cells may play a critical role in the cell-death process in the spinal cords of patients with sporadic and familial ALS.

Acknowledgments

This study was supported in part by a Grant-in-Aid from the Japan Society for the Promotion of Science (No. 20·10786).

References

Atkin, J.D., Farg, M.A., Turner, B.J., Tomas, D., Lysaght, J.A., Nunan, J., et al., 2006. Induction of the unfolded protein response in familial amyotrophic lateral sclerosis and association of protein-disulfide isomerase with superoxide dismutase 1. J. Biol. Chem. 281, 30152–30165.

Atkin, J.D., Farg, M.A., Walker, A.K., McLean, C., Tomas, D., Horne, M.K., 2008. Endoplasmic reticulum stress and induction of the unfolded protein response in human sporadic amyotrophic lateral sclerosis. Neurobiol. Dis. 30, 400–407.

Bassik, M.C., Scorrano, L., Oakes, S.A., Pozzan, T., Korsmeyer, S.J., 2004. Phosphorylation of BCL-2 regulates ER Ca^{2+} homeostasis and apoptosis. EMBO J. 23, 1207–1216.

Boillée, S., Yamanaka, K., Lobsiger, C.S., Copeland, N.G., Jenkins, N.A., Kassiotis, G., et al., 2006. Onset and progression in inherited ALS determined by motor neurons and microglia. Science 312, 1389–1392.

Breckenridge, D.G., Germain, M., Mathai, J.P., Nguyen, M., Shore, G.C., 2003. Regulation of apoptosis by endoplasmic reticulum pathways. Oncogene 22, 8608–8618.

Cleveland, D.W., Rothstein, J.D., 2001. From Charcot to Lou Gehrig: deciphering selective motor neuron death in ALS. Nat. Rev., Neurosci. 2, 806–819.

Eymin, B., Dubrez, L., Allouche, M., Solary, E., 1997. Increased GADD153 messenger RNA level is associated with apoptosis in human leukemic cells treated with etoposide. Cancer Res. 57, 686–695.

Fontanier-Razzaq, N.C., Hay, S.M., Rees, W.D., 1999. Upregulation of CHOP-10 (gadd153) expression in the mouse blastocyst as a response to stress. Mol. Reprod. Dev. 54, 326–332.

Gurney, M.E., Pu, H., Chiu, A.Y, Dal Canto, M.C., Polchow, C.Y., Alexander, D.D., et al., 1994. Motor neuron degeneration in mice that express a human Cu, Zn superoxide dismutase mutation. Science 264, 1772–1775.

Harding, H.P., Calfon, M., Urano, F., Novoa, I., Ron, D., 2002. Transcriptional and translational control in the mammalian unfolded protein response. Annu. Rev. Cell Dev. Biol. 18, 575–599.

Ilieva, E.V., Ayala, V., Jové, M., Dalfó, E., Cacabelos, D., Povedano, M., et al., 2007. Oxidative and endoplasmic reticulum stress interplay in sporadic amyotrophic lateral sclerosis. Brain 130, 3111–3123.

Jørgensen, M.M., Bross, P., Gregersen, N., 2003. Protein quality control in the endoplasmic reticulum. APMIS Suppl. 109, 86–91.

Kanekura, K., Suzuki, H., Aiso, S., Matsuoka, M., 2009. ER stress and unfolded protein response in amyotrophic lateral sclerosis. Mol. Neurobiol. 39, 81–89.

Kawahara, K., Mori, M., Nakayama, H., 2004. NO-induced apoptosis and ER stress in microglia. Nippon Yakurigaku Zasshi 124, 399–406.

Kieran, D., Woods, I., Villunger, A., Strasser, A., Prehn, J.H., 2007. Deletion of the BH3-only protein puma protects motoneurons from ER stress-induced apoptosis and delays motoneuron loss in ALS mice. Proc. Natl. Acad. Sci. U. S. A. 104, 20606–20611.

Kikuchi, H., Almer, G., Yamashita, S., Guégan, C., Nagai, M., Xu, Z., et al., 2006. Spinal cord endoplasmic reticulum stress associated with a microsomal accumulation of mutant superoxide dismutase-1 in an ALS model. Proc. Natl. Acad. Sci. U. S. A. 103, 6025–6030.

Lindholm, D., Wootz, H., Korhonen, L., 2006. ER stress and neurodegenerative diseases. Cell Death Differ. 13, 385–392.

Matsumoto, M., Minami, M., Takeda, K., Sakao, Y., Akira, S., 1996. Ectopic expression of CHOP (GADD153) induces apoptosis in M1 myeloblastic leukemia cells. FEBS Lett. 395, 143–147.

Maytin, E.V., Ubeda, M., Lin, J.C., Habener, J.F., 2001. Stress-inducible transcription factor CHOP/gadd153 induces apoptosis in mammalian cells via p38 kinase-dependent and -independent mechanisms. Exp. Cell Res. 267, 193–204.

Nagai, M., Aoki, M., Miyoshi, I., Kato, M., Pasinelli, P., Kasai, N., 2001. Rats expressing human cytosolic copper-zinc superoxide dismutase transgenes with amyotrophic lateral sclerosis: associated mutations develop motor neuron disease. J. Neurosci. 21, 9246–9254.

Nagai, M., Re, D.B., Nagata, T., Chalazonitis, A., Jessell, T.M., Wichterle, H., et al., 2007. Astrocytes expressing ALS-linked mutated SOD1 release factors selectively toxic to motor neurons. Nat. Neurosci. 10, 615–622.

Nagata, T., Ilieva, H., Murakami, T., Shiote, M., Narai, H., Ohta, Y., et al., 2007. Increased ER stress during motor neuron degeneration in a transgenic mouse model of amyotrophic lateral sclerosis. Neurol. Res. 29, 767–771.

Oyadomari, S., Mori, M., 2004. Roles of CHOP/GADD153 in endoplasmic reticulum stress. Cell Death Differ. 11, 381–389.

Oyanagi, K., Yamazaki, M., Takahashi, H., Watabe, K., Wada, M., Komori, T., et al., 2008. Spinal anterior horn cells in sporadic amyotrophic lateral sclerosis show ribosomal detachment from, and cisternal distention of the rough endoplasmic reticulum. Neuropathol. Appl. Neurobiol. 34, 650–658.

Park, E., Velumian, A.A., Fehlings, M.G., 2004. The role of excitotoxicity in secondary mechanisms of spinal cord injury: a review with an emphasis on the implications for white matter degeneration. J. Neurotrauma 21, 754–774.

Penas, C., Guzmán, M.S., Verdú, E., Forés, J., Navarro, X., Casas, C., 2007. Spinal cord injury induces endoplasmic reticulum stress with different cell-type dependent response. J. Neurochem. 102, 1242–1255.

Rao, R.V., Ellerby, H.M., Bredesen, D.E., 2004. Coupling endoplasmic reticulum stress to the cell death program. Cell Death Differ. 11, 372–380.

Ron, D., Habener, J.F., 1992. CHOP, a novel developmentally regulated nuclear protein that dimerizes with transcription factors C/EBP and LAP and functions as a dominant-negative inhibitor of gene transcription. Genes Dev. 6, 439–453.

Rosen, D.R., Siddique, T., Patterson, D., Figlewicz, D.A., Sapp, P., Hentati, A., et al., 1993. Mutations in Cu/Zn superoxide dismutase gene are associated with familial amyotrophic lateral sclerosis. Nature 362, 59–62.

Rutkowski, D.T., Kaufman, R.J., 2004. A trip to the ER: coping with stress. Trends Cell Biol. 14, 20–28.

Saxena, S., Cabuy, E., Caroni, P., 2009. A role for motoneuron subtype-selective ER stress in disease manifestations of FALS mice. Nat. Neurosci. [Electronic publication ahead of print].

Sekine, Y., Takeda, K., Ichijo, H., 2006. The ASK1-MAP kinase signaling in ER stress and neurodegenerative diseases. Curr. Mol. Med. 6, 87–97.

Szegezdi, E., Logue, S.E., Gorman, A.M., Samali, A., 2006. Mediators of endoplasmic reticulum stress-induced apoptosis. EMBO Rep. 7, 880–885.

Tobisawa, S., Hozumi, Y., Arawaka, S., Koyama, S., Wada, M., Nagai, M., et al., 2003. Mutant SOD1 linked to familial amyotrophic lateral sclerosis, but not wild-type SOD1, induces ER stress in COS7 cells and transgenic mice. Biochem. Biophys. Res. Commun. 303, 496–503.

Turner, B.J., Atkin, J.D., 2006. ER stress and UPR in familial amyotrophic lateral sclerosis. Curr. Mol. Med. 6, 79–86.

Vlug, A.S., Teuling, E., Haasdijk, E.D., French, P., Hoogenraad, C.C., Jaarsma, D., 2005. ATF3 expression precedes death of spinal motoneurons in amyotrophic lateral sclerosis-SOD1 transgenic mice and correlates with c-Jun phosphorylation, CHOP expression, somato-dendritic ubiquitination and Golgi fragmentation. Eur. J. Neurosci. 22, 1881–1894.

Wei, H., Kim, S.J., Zhang, Z., Tsai, P.C., Wisniewski, K.E., Mukherjee, A.B., 2008. ER and oxidative stresses are common mediators of apoptosis in both neurodegenerative and non-neurodegenerative lysosomal storage disorders and are alleviated by chemical chaperones. Hum. Mol. Genet. 17, 469–477.

Wootz, H., Hansson, I., Korhonen, L., Näpänkangas, U., Lindholm, D., 2004. Caspase-12 cleavage and increased oxidative stress during motoneuron degeneration in transgenic mouse model of ALS. Biochem. Biophys. Res. Commun. 322, 281–286.

Yamanaka, K., Yamashita, H., 2007. ALS and microglia-a player for non-cell-autonomous neuron death. Brain Nerve 59, 1163–1170.

Yamanaka, K., Boillee, S., Roberts, E.A., Garcia, M.L., McAlonis-Downes, M., Mikse, O.R., et al., 2008. Mutant SOD1 in cell types other than motor neurons and oligodendrocytes accelerates onset of disease in ALS mice. Proc. Natl. Acad. Sci. U. S. A. 105, 7594–7599.

Neuromuscular Disorders 19 (2009) 29–36

Contents lists available at ScienceDirect

Neuromuscular Disorders

journal homepage: www.elsevier.com/locate/nmd

Nuclear changes in skeletal muscle extend to satellite cells in autosomal dominant Emery-Dreifuss muscular dystrophy/limb-girdle muscular dystrophy 1B

Young-Eun Park [a], Yukiko K. Hayashi [a,*], Kanako Goto [a], Hirofumi Komaki [b], Yuichi Hayashi [c], Takashi Inuzuka [c], Satoru Noguchi [a], Ikuya Nonaka [a], Ichizo Nishino [a]

[a] Department of Neuromuscular Research, National Institute of Neuroscience, National Center of Neurology and Psychiatry, 4-1-1 Ogawa-higashi, Kodaira, 187-8502 Tokyo, Japan
[b] Department of Child Neurology, National Center Hospital of Neurology and Psychiatry, National Center of Neurology and Psychiatry, 4-1-1 Ogawa-higashi, Kodaira, 187-8551 Tokyo, Japan
[c] Department of Neurology and Geriatrics, Gifu University Graduate School of Medicine, 1-1 Yanagido, Gifu 501-1194, Japan

ARTICLE INFO

Article history:
Received 22 May 2008
Received in revised form 24 September 2008
Accepted 26 September 2008

Keywords:
Autosomal dominant Emery-Dreifuss muscular dystrophy (AD-EDMD)
Limb girdle muscular dystrophy type 1B (LGMD1B)
A-type lamins
Nucleus
Satellite cell
Pax7
MyoD
Regeneration

ABSTRACT

Autosomal forms of Emery-Dreifuss muscular dystrophy (AD-/AR-EDMD) and limb-girdle muscular dystrophy type 1B (LGMD1B) are caused by mutations in the gene encoding A-type lamins (*LMNA*). A-type lamins are major components of nuclear lamina and known to have important roles in maintaining nuclear integrity. *LMNA* mutations are also suggested to cause reduced myogenic differentiation potentials, implying that satellite cell nuclei in AD-EDMD/LGMD1B are likewise affected. We examined nuclear changes of skeletal muscles including satellite cells from four patients with AD-EDMD/LGMD1B by light and electron microscopy. We found that 92.5 ± 5.0% of myonuclei had structural abnormalities, including shape irregularity and/or chromatin disorganization, and the presence of peri-/intranuclear vacuoles. Chromatin changes were also observed in 50% of the satellite cell nuclei. Increased number of Pax7-positive nuclei, but fewer number of MyoD-positive nuclei were seen on immunohistochemical analyses, suggesting functional alteration of satellite cells in addition to the nuclear morphological changes in AD-EDMD/LGMD1B.

1. Introduction

Autosomal dominant and recessive forms of Emery-Dreifuss muscular dystrophy (AD- and AR-EDMD, respectively) are caused by the mutations in the *LMNA* gene that encodes A-type lamins, and are clinically characterized by muscle weakness with humeroperoneal distribution, early onset joint contractures and dilated cardiomyopathy with conduction defects [1]. *LMNA* mutations can also cause limb-girdle muscular dystrophy type 1B (LGMD1B), which has the clinical feature of proximal dominant muscle weakness with cardiac involvement [2].

Lamins form the nuclear lamina meshwork at the inner nuclear membrane and are suggested to have an important role in the maintenance of nuclear architecture. *LMNA* mutations or *Lmna* knockout are proven to cause nuclear dysmorphism and increase the fragility against mechanical stress in cultured cell analyses [3,4], supporting the notion that the nuclear lamina holds nuclear integrity. From this concept, myonuclei are presumably affected when *LMNA* is mutated since the skeletal muscle is frequently exposed to strong mechanical stress through the process of muscle contraction and relaxation. *LMNA* mutations were also shown to cause altered differentiation potential and kinetics of skeletal muscle cells by *in vitro* cell analyses [5].

In this study, we examined the morphological changes of myonuclei, and also nuclei of satellite cells in the skeletal muscles from four patients with genetically confirmed AD-EDMD/LGMD1B by using light and electron microscope. Further, we also counted the number of the myonuclei expressing Pax7 and MyoD to evaluate the differentiation potential of satellite cells in AD-EDMD/LGMD1B.

2. Patients and methods

2.1. Patients

All clinical materials used in this study were obtained for the diagnostic purposes with informed consent. Clinical information of four patients with AD-EDMD/LGMD1B is summarized in Table 1. In brief;

* Corresponding author. Tel.: +81 42 341 2711; fax: +81 42 346 1742.
E-mail address: hayasi_y@ncnp.go.jp (Y.K. Hayashi).

0960-8966/$ - see front matter © 2008 Elsevier B.V. All rights reserved.
doi:10.1016/j.nmd.2008.09.018

Patient 1 is a 4-year and 5-month-old girl who was clinically suspected to have LGMD. She presented with lordosis and waddling gait from the age of 2 years. On physical examination, she showed proximal limb muscle weakness with wasting and calf hypertrophy. Serum creatine kinase (CK) level was elevated to 1408 IU/L (normal: 51–197 IU/L). Sequence analysis of *LMNA* revealed a heterozygous mutation of c.1357C > T (p.R453W) in exon 7.

Patient 2 is a 5-year and 8-month-old girl, who was noticed to have limited ankle flexion and elevation of serum CK level at the age of 2 years. On admission, she showed generalized muscle wasting, lordosis, and ankle/knee joint contractures. Serum CK levels were elevated from 900 to 1500 IU/L. The presence of a heterozygous mutation of c.746G > A (p.R249Q) in exon 4 of *LMNA* confirmed the diagnosis of EDMD.

Patient 3 is an 8-year and 1-month-old girl who had muscle weakness and delayed motor milestones. She walked without support at the age of 1 year and 4 months, but gradually lost independent ambulation at around 3 years of age. Scoliosis was noted on physical examination. Serum CK level was 351 IU/L. Echocardiography showed mildly decreased cardiac motility. Genetic analysis revealed a heterozygous missense mutation of c.875T > C (p.L292P) in exon 5 of *LMNA*.

Table 1
Clinical and genetic information of four patients with AD-EDMD/LGMD1B.

	Patient 1	Patient 2	Patient 3	Patient 4
Age/Sex	4 years/F	5 years/F	8 years/F	52 years/F
Age at onset	2 years	2 years	1 year 4 months	6 years
Skeletal muscle symptoms	Prox. limb weakness Lordosis Calf hypertrophy	Prox. limb weakness Lordosis	Prox. limb weakness Scoliosis Loss of ambulation	Prox. limb weakness Facial/neck weakness
Joint contracture	None	Ankles & knees	None	None
Cardiac symptoms	None	None	Wall motion decrease on echocardiography	Sick sinus syndrome + ventricular tachycardia → pacemaker insertion
Serum CK (IU/L)	1408	900–1500	351	117
LMNA mutation	p.R453W	p.R249Q	p.L292P	p.D511fs

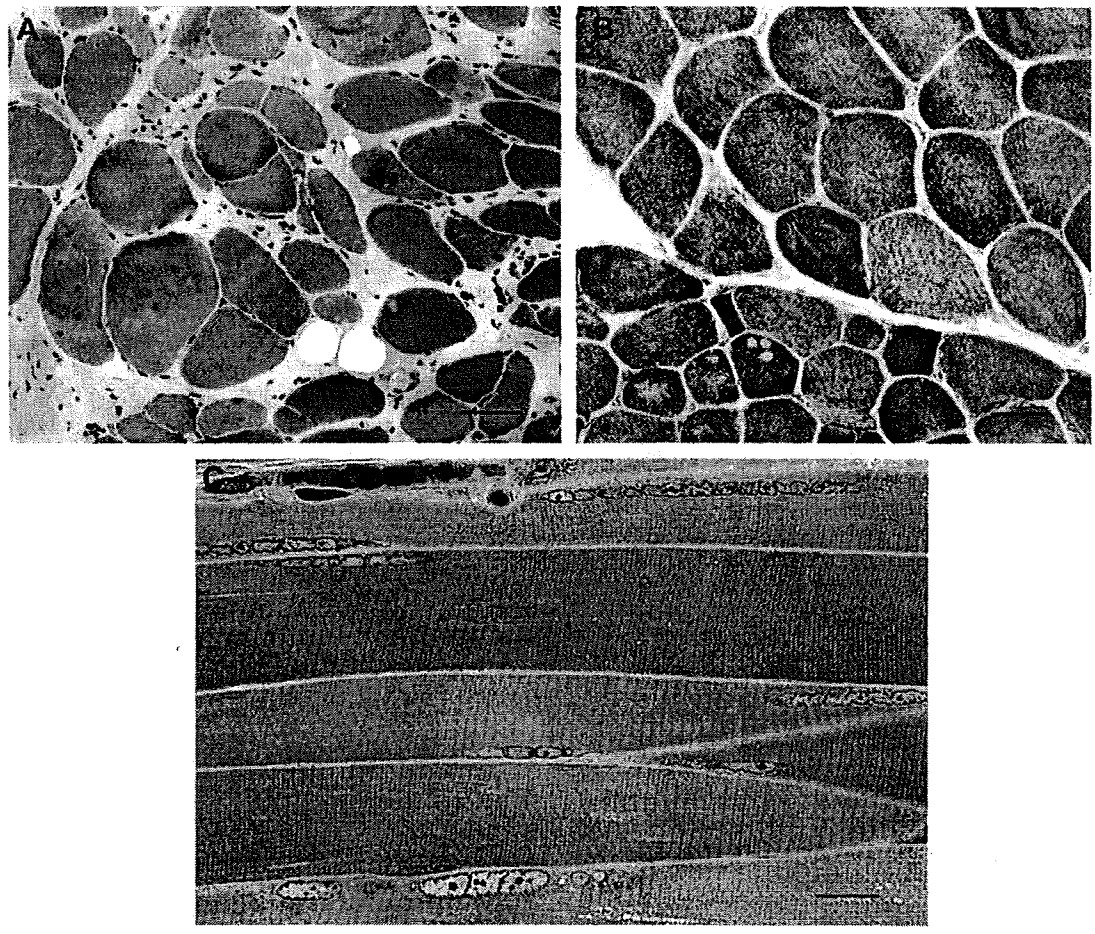

Fig. 1. Light microscopic observation of skeletal muscle. (A) H&E staining in patient 3 shows that the number of nuclei within one fiber is markedly increased. (B) NADH staining in patient 4 shows well-preserved myofibril organization in many fibers, whereas a few fibers have core/mini core-like structure. (C) Semi-thin section in patient 1 stained by toluidine blue contains nuclear chains of variable size in subsarcolemmal regions. Bar = 100 μm (A and B), 50 μm (C).

Patient 4 is a 52-year-old female, whose family history was suggestive of an autosomal dominant inheritance because her mother and her mother's sister had muscle weakness and cardiac enlargement/arrhythmia. She had been a slow runner since childhood and waddling gait was noticed at the age of 6 years. She felt difficulty in climbing stairs from 35 years of age. A diagnosis of sick sinus syndrome with ventricular tachycardia was given at 46 years whereby a pacemaker was inserted. Serum CK level was 117 IU/L. Mutation analysis showed a novel heterozygous frame-shift mutation of c.1527-1529TAC < AA (p.D511fs) in exon 9 of *LMNA*.

For comparison of histochemical and immunohistochemical analyses, muscle specimen from age-matched patients with Duchenne/Becker muscular dystrophy (DMD/BMD) ($n = 4$) and normal controls ($n = 4$) were also analyzed.

2.2. Histochemical analyses

Biopsied muscle specimens were flash-frozen in isopentane chilled with liquid nitrogen. Serial 10 μm-thick frozen sections were analyzed with a set of histochemical staining including hematoxylin and eosin (H&E), modified Gomori trichrome, nicotinamide adenine dinucleotide-tetrazolium reductase (NADH-TR), succinate dehydrogenase (SDH), cytochrome *c* oxidase and myosin ATPase. On ATPase staining, the ratio of type 2C fibers was considered in the patients with AD-EDMD/LGMD1B, and age-matched Duchenne/Becker muscular dystrophy (DMD/BMD) and normal controls.

2.3. Immunohistochemical analysis

Serial 6 μm-thick frozen muscle sections were fixed with acetone. Immunostaining was performed using standard method. To exclude other diagnosable muscular dystrophies, we used antibodies against dystrophin (Dys1, Dys2, and Dys3 from Novocastra Laboratories, Newcastle upon Tyne, UK), α-dystroglycan (Upstate Biotechnology, Lake Placid, NY), β-dystroglycan (Novocastra Laboratories), dysferlin (Novocastra Laboratories), α-, β-, γ-, δ-sarcoglycan (Novocastra Laboratories), caveolin-3 (Novocastra Laboratories), laminin-α2 chain (Chemicon, Temecula, CA), collagen VI (Abcam, Cambridge, UK), emerin (Novocastra Laboratories), and lamin A/C (Abcam, Tokyo, Japan).

For the satellite cell analyses, primary antibodies against Pax7 (Developmental Studies Hybridoma Bank, The University of Iowa, IA), MyoD (Santa Cruz Biotechnology, CA), and laminin α2 (Chemicon) were used. The stained sections were mounted together with DAPI for nuclear localization, and examined under immunofluorescence microscope (Carl Zeiss). In this study, immunopositive nuclei for Pax7 or MyoD located beneath the laminin α2-positive basal lamina are defined as Pax7-positive or MyoD-positive. From each specimen, 200–300 nuclei were recruited for analyses. The number of Pax7-positive or MyoD-positive nuclei was counted and compared with the total number of myonuclei to obtain the ratio of Pax7 and MyoD-positive nuclei per 100 myonuclei.

To detect DNA fragmentation, the TUNEL method was performed on frozen muscle specimens by using in situ apoptosis detection kit (Takara, Shiga, Japan) according to the manufacturer's instruction.

2.4. Electron microscopic observation

Muscle specimens were fixed with 2% glutaraldehyde in 0.1 M cacodylate buffer. After shaking with a mixture of 4% osmium tetroxide, 1.5% lanthanum nitrate, and 0.2 M s-collidine for 2–3 h, samples were embedded in epoxy resin. Semi-thin sections (1 μm-thickness) were stained with toluidine blue. Ultrathin sections of 50 nm thickness were stained with uranyl acetate and lead citrate, and then examined under H-600 transmission electron microscope (Hitachi, Japan) at 75 kV. We examined morphological changes of more than 100 myonuclei in each patient and 100 myonuclei in one DMD patient as a control. We also examined 20 satellite cell nuclei in each patient. Myonuclei in significantly degenerated myofibers were excluded from the count. We calculated the frequency of myonuclei showing markedly irregular membrane contours and nuclear chains. We also counted the number of nuclei having only thin heterochromatin (scanty heterochromatin) beneath the nuclear membrane. Mean percentage ± standard deviation (SD) of abnormal nuclei was calculated. To detect the euchromatin changes, intensities of photocopied euchromatin regions in randomly sampled 40 nuclei of each patient and a DMD control were measured by using Photoshop. We

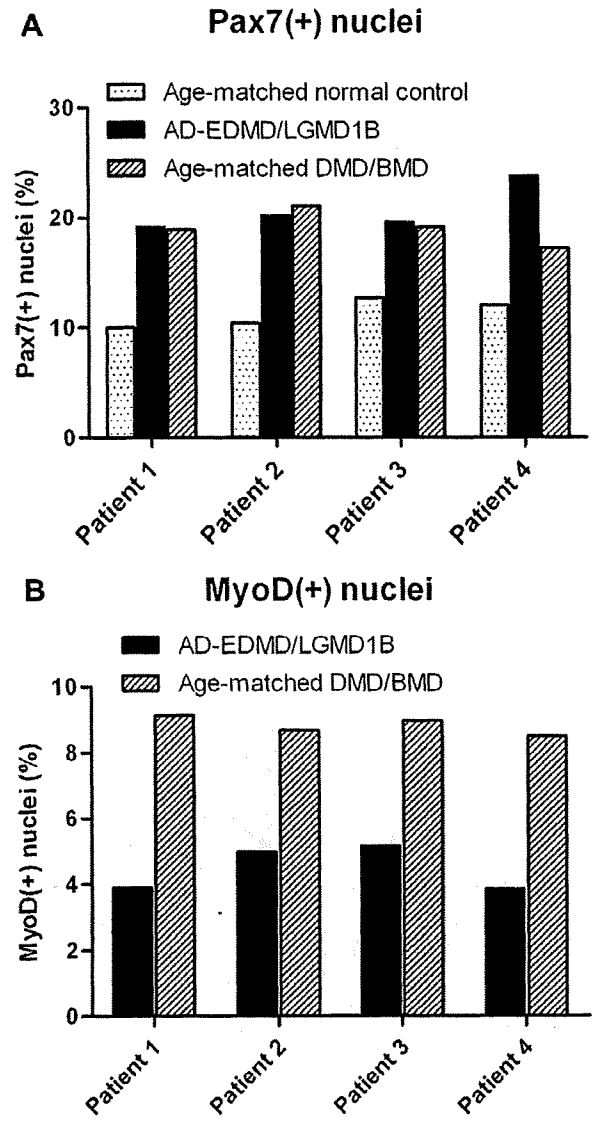

Fig. 2. Graphs showing the ratio of Pax7-positive (A) and MyoD-positive nuclei (B) in the patients with AD-EDMD/LGMD1B, and age-matched DMD/BMD and normal controls. (A) The ratio of Pax7-positive nuclei is increased both in AD-EDMD/LGMD1B and DMD/BMD patients compared with normal controls. (B) MyoD-positive nuclei in AD-EDMD/LGMD1B patients are much less than in DMD/BMD patients.

randomly chose three spots of 0.09 μm^2 in euchromatin region per each nucleus and calculate the mean intensity. To normalize the intensity of each photocopy, we used the mean intensity of three spots in A-band (excluded M-line region) of well-preserved sarcomere close to the nucleus as control. We defined as 'coarse euchromatin' when the nucleus has higher intensity (less electron dense) of euchromatin than mean plus SD of euchromatin intensity in DMD muscle. *P*-value was calculated using One-way ANOVA test.

3. Results

3.1. Histochemical analyses

Biopsied muscles from all four patients showed marked variation in fiber size, a few necrotic and regenerating fibers and mild to moderate endomysial fibrosis, which were compatible with the diagnosis of muscular dystrophy. The number of muscle fibers with internalized nuclei was increased. Interestingly, the number

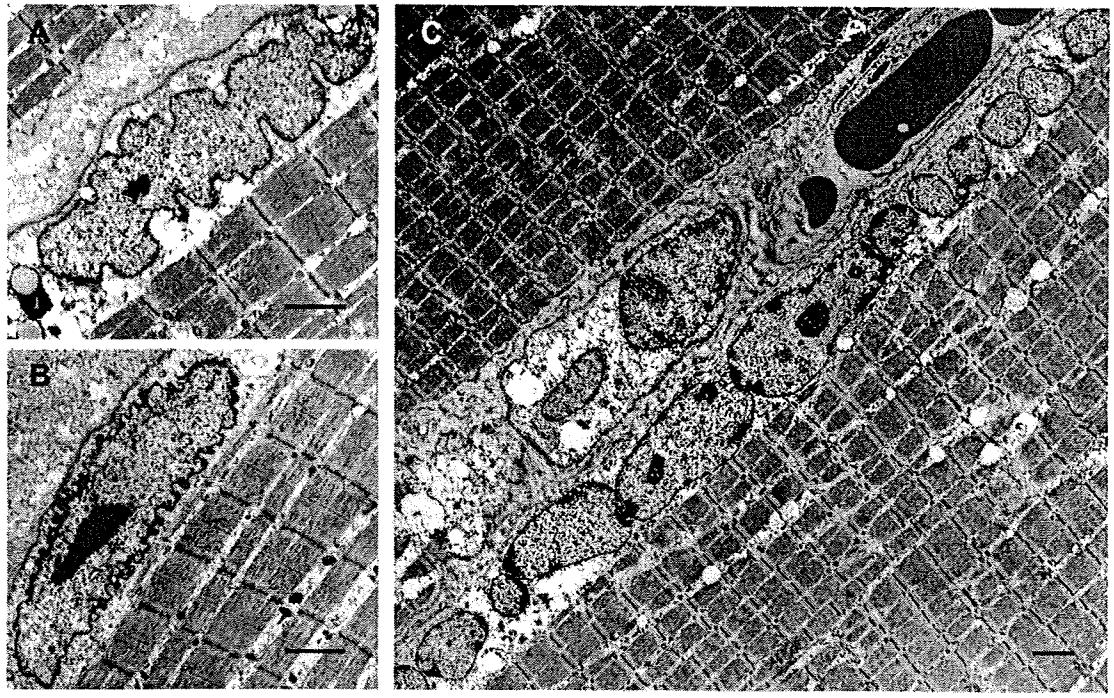

Fig. 3. Changes in the shape of myonucleus from patient 4 (A and B) and patient 1 (C). (A and B) Nuclear contours are irregular showing serpentine and sawtooth-like features. (C) A nuclear chain is identified in subsarcolemmal region, which is corresponded to those in the semi-thin section of Fig. 1C. Bar = 1 μm.

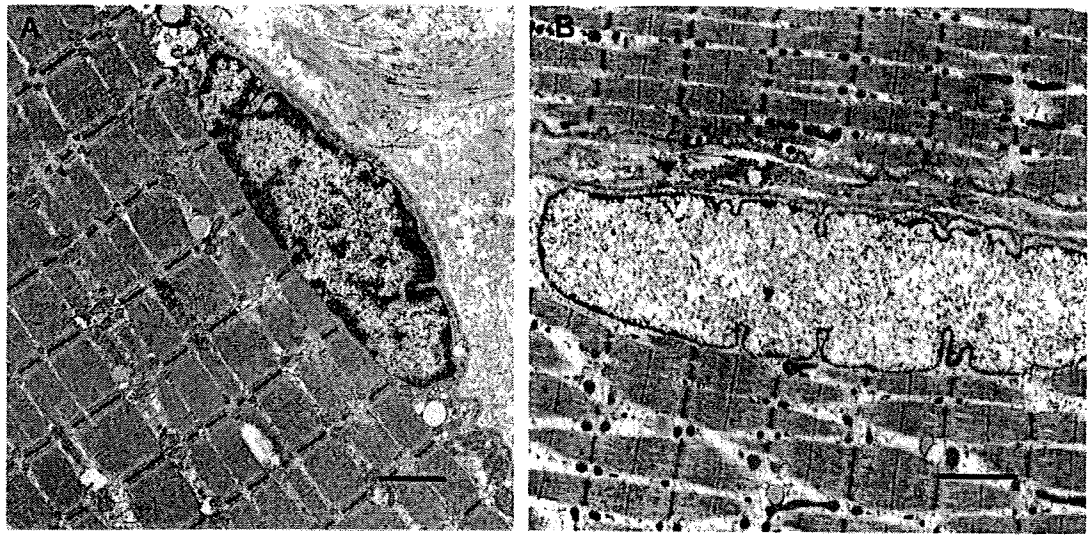

Fig. 4. Chromatin organization in myonuclei from one DMD control (A) and patient 4 (B). (A) Myonucleus of DMD has abundant heterochromatin and condensed euchromatin. (B) In myonucleus of the patient with AD-EDMD/LGMD1B, heterochromatin was scanty or nearly absent, and euchromatin reveals reduced density and coarse texture. Bar = 1 μm.

of nuclei contained in one muscle fiber was markedly increased, sometimes exceeding ten in number (Fig. 1A). The organization of intermyofibrillar networks was not disrupted in three of the patients, but in a restricted area of muscle in patient 4, myofibril disorganization was seen in a few fibers on NADH-TR showing core/minicore-like structures (Fig. 1B). On ATPase staining, type 2C fibers comprised 7.8 ± 1.5% in the patients with AD-EDMD/LGMD1B, and this value was slightly higher than in age-matched DMD/BMD controls (6.8 ± 0.9%). In age-matched normal controls, type 2C fibers were less than 1%.

Longitudinal semi-thin sections from epoxy resin-embedded blocks also showed nuclei in the center of myofibers, as well as subsarcolemmal regions. Some myonuclei had pale-colored nucleoplasm making nucleoli more distinct. Notably, several smaller-sized nuclei were arranged in a row giving a feature of the 'nuclear chain' on longitudinal sections, and most of them were located in the subsarcolemmal regions (Fig. 1C).

3.2. Immunohistochemical analysis

The immunostaining of various antibodies as described above excluded all other diagnosable muscular dystrophies. In all four patients with AD-EDMD/LGMD1B and DMD patients examined, only few TUNEL-positive myonuclei were seen (data not shown). This result suggests that apoptotic nuclear change is rare in AD-EDMD/LGMD1B.

In satellite cell analyses, the ratio of Pax7-positive nuclei in the patients with AD-EDMD/LGMD1B, DMD/BMD patients, and normal controls were 20.7 ± 2.1%, 19.1 ± 1.6% and 11.3 ± 1.3%, respectively (Fig. 2A). The ratio of Pax7-positive nuclei in each patient with AD-EDMD/LGMD1B were similar to those in the age-matched DMD/BMD controls except for patient 4 who showed more increased number of Pax7-positive nuclei. In contrast, the ratio of MyoD-positive nuclei was lower in AD-EDMD/LGMD1B (4.5 ± 0.7%) than in DMD/BMD (8.8±0.3%) (Fig. 2B).

3.3. Electron microscopic observation

Abnormalities in the nuclear morphology were the major findings on electron microscope in all four patients with AD-EDMD/LGMD1B, and which were virtually absent in the DMD patient examined. We have focused on the changes in nuclear shape and chromatin organization, and the presence of peri- and intranuclear vacuoles.

The shape of myonuclei was altered in all four patients with AD-EDMD/LGMD1B; 17.3 ± 11.1% of myonuclei displayed markedly irregular membrane contours, such as serpentine or sawtooth-like features (Fig. 3A and B). In addition, nuclear chains corresponding to those seen in semi-thin sections were identified in subsarcolemmal regions, accounting for 18.5 ± 6.4% of the myonuclei (Fig. 3C). In contrast, almost all myonuclei in the DMD patient had smooth-contoured nuclear membranes albeit mild indentation.

Another nuclear abnormality noted was chromatin disorganization in the myonuclei. In the myonuclei of DMD patient, heterochromatin appears abundant in the nuclear periphery and euchromatin is well-condensed in the nuclear interior (Fig. 4A). On the other hand, 64.3 ± 18.5% of the myonuclei in AD-EDMD/LGMD1B had only thin layer of heterochromatin under the inner nuclear membrane (scanty heterochromatin), and some of them showed totally absent heterochromatin (Fig. 4B). In addition, euchromatin appeared coarse and had reduced electron density as compared with myonuclei in DMD (Fig. 4B). Mean euchromatin intensities in all four patients were significantly higher than DMD ($P < 0.001$) (Supplemental Fig.), and 75.0 ± 16.7% of nuclei had higher euchromatin intensity than mean + SD of DMD.

More importantly, chromatin organization of the satellite cell nuclei were also affected (Fig. 5). Although only twenty satellite cells were observed in each patient, nearly a half of them contained the nuclei with scanty heterochromatin, and less condensed and coarse euchromatin, features of which are quite similar to those seen in the myonuclei. In spite of chromatin disorganization, however, the nuclear shape was well preserved in the satellite cells.

Another finding associated with the myonuclei of the four patients is the presence of peri- and intranuclear vacuoles, which were observed in ~10% of the myonuclei. Most of these vacuoles were variable in size and contained various materials within, but the larger intranuclear vacuoles were mostly empty (Fig. 6). All the myonuclei with vacuoles were basically abnormal in shape and/or chromatin organization as shown in Fig. 6.

The perinuclear vacuoles were observed in close proximity to the myonuclei; for example, in the poles or in deeply indented por-

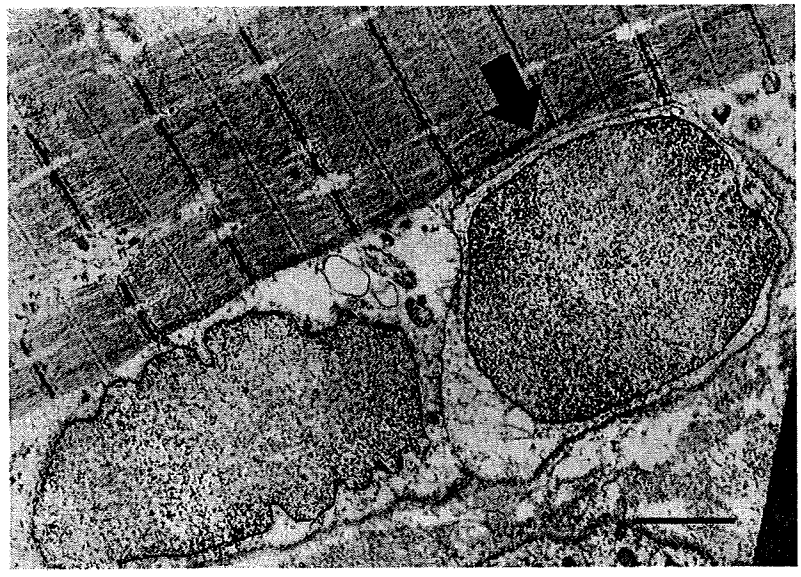

Fig. 5. Chromatin disorganization of satellite cell nuclei from patient 4. Arrow indicates the satellite cell having abnormal chromatin texture of nucleus, which is similar to that seen in myonucleus. Bar = 1 μm.

tion of the myonuclei (Fig. 6A and B). Several perinuclear vacuoles were almost attached to the myonuclei, so that the border of each membrane was indistinguishable (Fig. 6A). Specifically, the outer nuclear membrane of some with perinuclear vacuoles was partially separated from the inner membrane giving a visible gap between the two membranes (Fig. 6B).

Intranuclear vacuoles were observed in obviously degenerated myonuclei which have highly condensed chromatin structures (Fig. 6C and D). Of note, the larger intranuclear vacuoles occupied a significant portion of the intranuclear area leaving only a little space of compact chromatin, and these myonuclei were usually placed in the markedly degenerated myofibers (Fig. 6D). Nevertheless, general myofibrillar organization was relatively well preserved in most part of myofibers, except for only limited regions close to the altered myonuclei showing a Z-line streaming or myofibril derangement (Fig. 7).

Overall, 92.5 ± 5.0% of the myonuclei had abnormality in shape and/or chromatin organization. However, the proportion of abnormal myonuclei was similar from the youngest to the adult patient, with no correlation to the patients' age at biopsy, clinical severity or the location of mutations in *LMNA* (Fig. 8).

4. Discussion

We characterized the nuclear changes in the skeletal muscles of AD-EDMD/LGMD1B caused by *LMNA* mutations. The nuclear lamina is expected to function as a scaffold of the nucleus, thus nuclear fragility due to *LMNA* mutations is regarded as one of the patho-

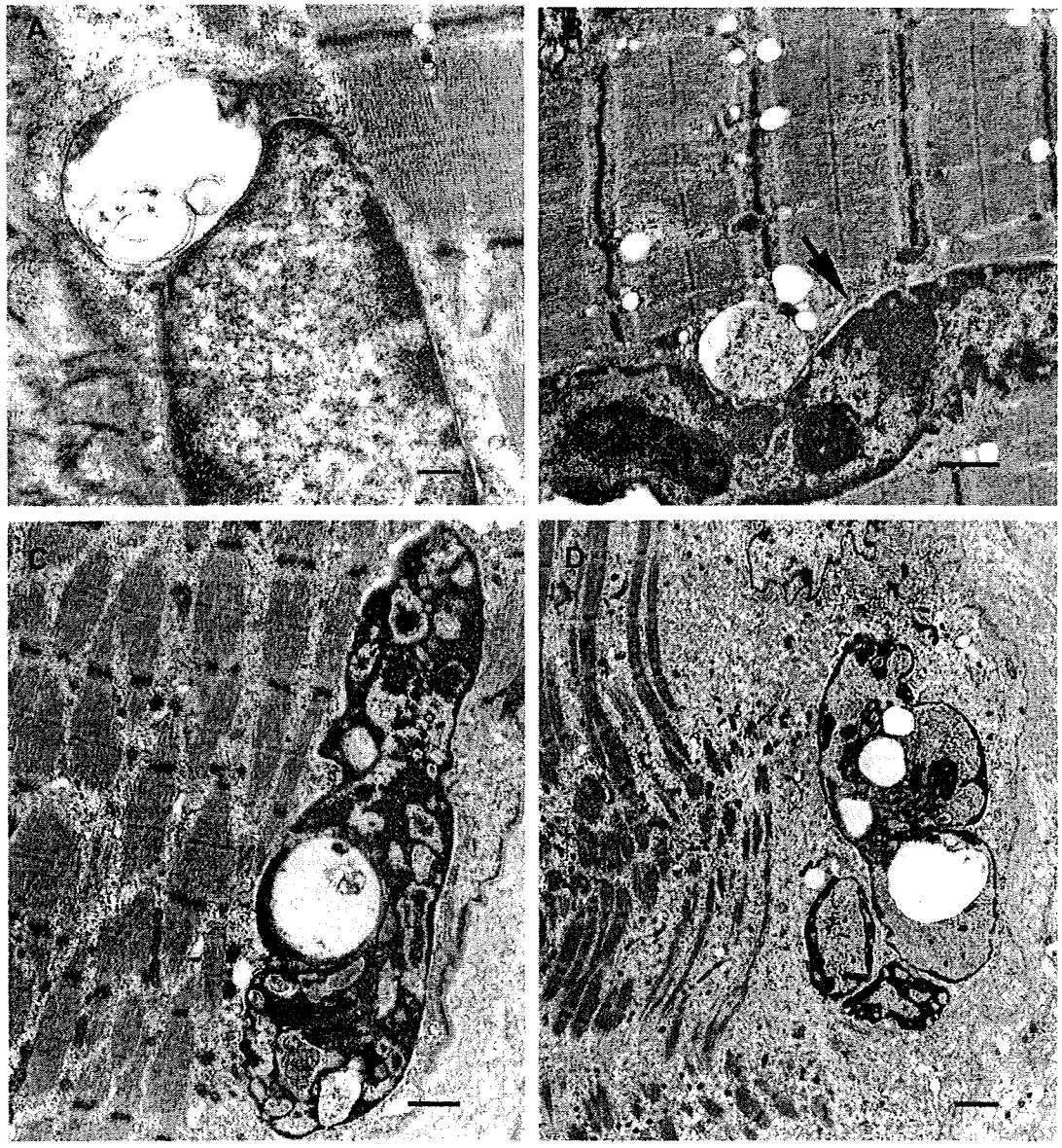

Fig. 6. Perinuclear and intranuclear vacuoles of myonuclei in patient 1 (A and B), patient 4 (C) and patient 3 (D). Vacuoles contain various materials (A, B and C), but larger intranuclear vacuoles are empty (D). (A) Nuclear membrane is difficult to be distinguished from the membrane of perinuclear vacuole. (B) Inner and outer nuclear membranes are partially separated from each other, as indicated by an arrow, in the myonucleus with perinuclear vacuoles. (C) Intranuclear vacuole is seen in quite degenerated myonucleus with highly condensed chromatin. (D) Intranuclear vacuoles occupy significant portion of intranuclear area leaving only small spaces for disorganized chromatin. Myofibrils surrounding the myonucleus were markedly degenerated. Bars = 0.2 μm (A), 0.5 μm (B and C), 1 μm (D).

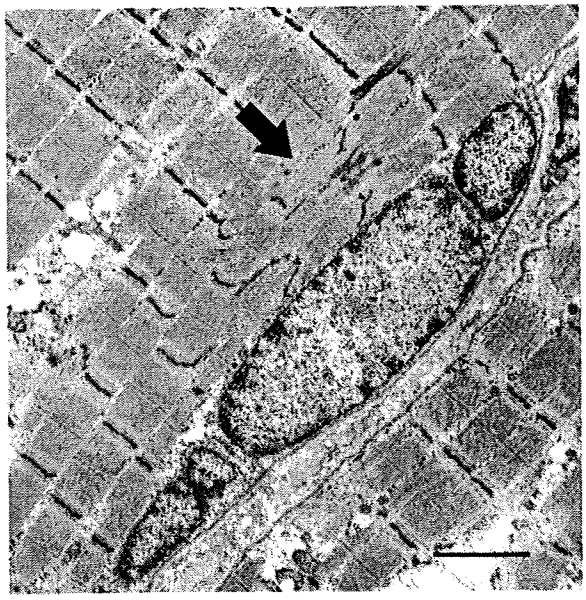

Fig. 7. In a few fibers in patient 4, myofibrils were disorganized in the region close to the altered myonucleus showing Z-line streaming as indicated by an arrow. Bar = 1 μm.

mechanism in laminopathy. In support of this concept, nuclear dysmorphism and vulnerability to mechanical stress were reported in cultured fibroblasts from *Lmna*-null mice [3,4] and the patients with *LMNA* mutations [6,7]. In this study, we demonstrated that the myonuclei of AD-EDMD/LGMD1B patients had markedly irregular nuclear membrane contours. Our findings are in agreement to previous reports which showed that the AD-EDMD/LGMD1B patients had irregularly shaped nuclei, such as convoluted, segmented and fragmented features [8–10]. These data with myonuclei provide additional evidence of nuclear fragility induced by *LMNA* mutations.

The presence of nuclear chain, which has not been previously described in AD-EDMD/LGMD1B, is worth mentioning, as it has been described almost as a pathognomonic feature of myotonic dystrophy [11], although nuclear chains can be seen in other neuromuscular disorders. The difference on these nuclear chains in AD-EDMD/LGMD1B is that they are found mostly in the subsarcolemmal area, while those in myotonic dystrophy were usually seen in the center of myofibers. Although the comparison is difficult because nuclear chains observed in myotonic dystrophy have not been well characterized by electron microscope, each disorder might have different mechanism forming nuclear chains. Similar nuclear chains were seen in the skeletal muscles of X-linked recessive EDMD (X-EDMD) under light microscope (data not shown). X-EDMD is caused by the mutations in the gene encoding emerin (*EMD*), which is another nuclear envelope protein [12] that directly associates to the nuclear lamina [13]. Based on these findings, nuclear chain formation, together with irregular nuclear shape, can be thought to result from the fragility of nuclear envelope.

Chromatin disorganization characterized by scanty heterochromatin and less condensed euchromatin, was also highlighted in our study. Previously, Sabatelli et al. have described the absence of heterochromatin and de-condensed euchromatin in about 10% of the myonuclei in AD-EDMD/LGMD1B [8]. Fidzianska and Hausmanowa-Petrusewicz also reported dark and dense heterochromatin in the myonuclei of AD-EDMD [9]. These chromatin changes observed in AD-EDMD/LGMD1B could correspond to the fact that nuclear lamins have an important role in the chromatin organization [14].

The presence of peri-/intranuclear vacuoles is a novel finding in this study, and is indeed a constant feature in all AD-EDMD patients we examined. We have previously reported similar perinuclear vacuoles in emerin-deficient mice [15], suggesting that these vacuoles can be one of the common characteristic pathological features in nuclear envelopathies including laminopathy and emerinopathy. Because perinuclear vacuoles were closely associated with nuclear membrane, and intranuclear vacuoles were found in quite distorted myonuclei having irregular shape and compact chromatin, we hypothesize that these could be secondary changes to the altered nuclear envelope. However, further experiment should be performed to characterize how these vacuoles are formed and how they contribute to the overall pathomechanism of laminopathy and emerinopathy.

Notably, we did not find any correlation of the degree of nuclear changes with the patients' age at biopsy, clinical severity and the location of mutations in the gene. Furthermore, even in the youngest patient the nuclear changes in shape and chromatin organization were already developed in a significant portion of the myonuclei as seen in Fig. 8, which can imply that the nuclear abnormality in patients with *LMNA* mutations occur at a much younger age than expected.

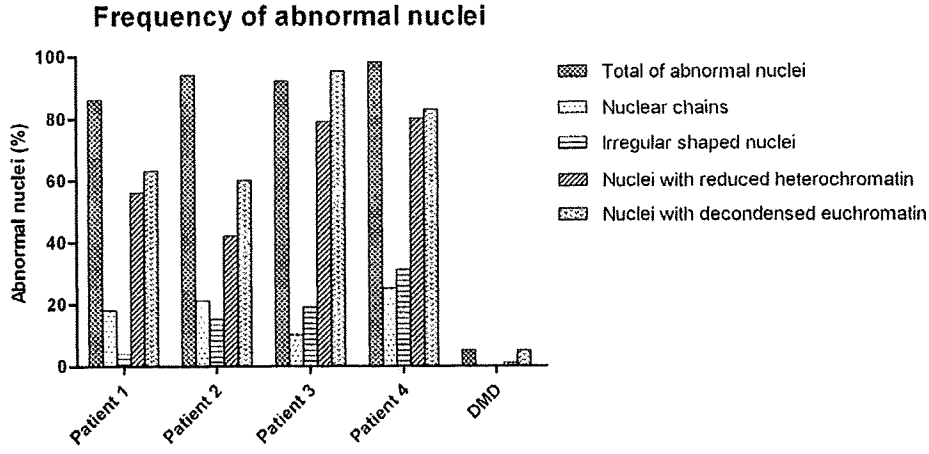

Fig. 8. The frequency of myonuclear abnormalities in four patients with AD-EDMD/LGMD1B and one DMD patient. Various kinds of nuclear changes are observed in high frequency in muscles from all four patients with AD-EDMD/LGMD1B. These changes are not correlated with the patients' age at biopsy, clinical severity and the location of mutations in the gene. Nuclear changes in a DMD muscle used as control are rare.

Recent reports suggested that decreased differentiation potential might be associated with muscular dystrophy caused by *LMNA* mutations. Favreau et al. reported that C2C12 myoblasts expressing the mutant (R453W) lamin A failed to form multinucleated fibers and were unable to express the myogenic transcriptional factor, myogenin, at proper timepoint during differentiation process [5]. Moreover, the mutant lamins induce the persistence of hyperphosphorylated Rb, preventing cell cycle arrest. Similarly, Bakay et al. revealed that the Rb-MyoD pathway of muscle regeneration is disrupted in nuclear envelope muscular dystrophies [16]. Furthermore, in *Lmna*$^{-/-}$ mouse, satellite cells showed delayed differentiation kinetics due to loss of A-type lamins [17]. Collectively these data raise the possibility that the skeletal muscle satellite cells in AD-EDMD/LGMD1B are likewise affected. As described in electron microscopic observation, the satellite cell nuclei show disorganized chromatin, and are indeed affected by *LMNA* mutations. The chromatin changes in satellite cell nuclei and myonuclei appeared to be quite similar, further providing the evidence that mutant lamins can influence chromatin organization even in the satellite cell nuclei.

A large number of type 2C fibers indicate the presence of immature fibers to be further differentiated. High composition of type 2C fiber in DMD/BMD muscles can be reflective of active regeneration following to muscle fiber necrosis. On the other hand, similar or rather higher composition of type 2C fibers with fewer necrotic fibers in the skeletal muscles of AD-EDMD/LGMD1B than DMD/BMD might indicate delayed completion of regeneration process. Altered chromatin organization observed in the satellite cells might have certain effects on transcriptional regulation in AD-EDMD/LGMD1B.

To evaluate the satellite cell functions, we examined Pax7 and MyoD expression in skeletal muscles. The number of Pax7-positive nuclei was increased to the similar extent in both AD-EDMD/LGMD1B and DMD/BMD compared with the age-matched normal controls. On the other hand, MyoD-positive nuclei were less pooled in AD-EDMD/LGMD1B than DMD/BMD.

In response to stimuli such as muscle injury, mechanical loading and denervation, satellite cells proliferate and a part of them terminally differentiate into myogenic cells [18]. The quiescent satellite cells express the transcriptional factor of Pax7, and when activated they proliferate and co-express Pax7 and MyoD, and after this, muscle differentiation is thought to progress with the down-regulation of Pax7 [19]. Increased number of both Pax7-positive and MyoD-positive nuclei observed in DMD/BMD patients indicates the activation and proliferation of satellite cells, as reported in dystrophin-deficient *mdx* mice [20]. Different from the condition of DMD/BMD, much smaller population of MyoD-positive nuclei in AD-EDMD/LGMD1B might reflect insufficient differentiation/regeneration process of skeletal muscle, even with similarly increased Pax7-positive satellite cells. These results are also consistent with the previous data which demonstrated markedly reduced (<60%) level of MyoD but preserved levels of Pax7 and MEF2 in *Lmna*$^{-/-}$ myoblasts [17]. In AD-EDMD/LGMD1B patients, the genes associated with muscle differentiation might also be affected resulting in delayed muscle regeneration. Further examination is needed to elucidate the roles of chromatin disorganization in the gene expression related to muscle differentiation.

In conclusion, our results demonstrate that *LMNA* mutations can make various kinds of nuclear abnormalities both in myonuclei and satellite cell nuclei, further supporting the role of A-type lamins in the maintenance of nuclear integrity. In addition, our results show that the skeletal muscle regeneration might be delayed due to decreased differentiation potential of the satellite cells in AD-EDMD/LGMD1B.

Acknowledgements

We thank Dr. May Christine V. Malicdan (National Institute of Neuroscience, NCNP) for reviewing the manuscript. This study was supported by "Research on Psychiatric and Neurological Diseases and Mental Health" of "Health Labour Sciences Research Grant" and the "Research Grant for Nervous and Mental Disorders" from the Ministry of Health, Labor, and Welfare; by grants from the Human Frontier Science Program; by a Grant-in-Aid for Scientific Research from Japan Society for the Promotion of Science; by Research on Publicly Essential Drugs and Medical Devices from the Japanese Health Sciences Foundation; and by the Program for Promotion of Fundamental Studies in Health Sciences of the National Institute of Biomedical Innovation (NIBIO).

Appendix A. Supplementary data

Supplementary data associated with this article can be found, in the online version, at doi:10.1016/j.nmd.2008.09.018.

References

[1] Bonne G, Di Barletta MR, Varnous S, et al. Mutations in the gene encoding lamin A/C cause autosomal dominant Emery-Dreifuss muscular dystrophy. Nat Genet 1999;21:285–8.
[2] Muchir A, Bonne G, van der Kooi AJ, et al. Identification of mutations in the gene encoding lamins A/C in autosomal dominant limb girdle muscular dystrophy with atrioventricular conduction disturbances (LGMD1B). Hum Mol Genet 2000;9:1453–9.
[3] Sullivan T, Escalante-Alcalde D, Bhatt H, et al. Loss of A-type lamin expression compromises nuclear envelope integrity leading to muscular dystrophy. J Cell Biol 1999;147:913–20.
[4] Lammerding J, Schulze PC, Takahashi T, et al. Lamin A/C deficiency causes defective nuclear mechanics and mechanotransduction. J Clin Invest 2004;113:370–8.
[5] Favreau C, Higuet D, Courvalin JC, Buendia B. Expression of a mutant lamin A that causes Emery-Dreifuss muscular dystrophy inhibits in vitro differentiation of C2C12 myoblasts. Mol Cell Biol 2004;24:1481–92.
[6] Muchir A, van Engelen BG, Lammens M, et al. Nuclear envelope alterations in fibroblasts from LGMD1B patients carrying nonsense Y259X heterozygous or homozygous mutation in lamin A/C gene. Exp Cell Res 2003;291:352–62.
[7] Muchir A, Medioni J, Laluc M, et al. Nuclear envelope alterations in fibroblasts from patients with muscular dystrophy, cardiomyopathy, and partial lipodystrophy carrying lamin A/C gene mutations. Muscle Nerve 2004;30:444–50.
[8] Sabatelli P, Lattanzi G, Ognibene A, et al. Nuclear alterations in autosomal-dominant Emery-Dreifuss muscular dystrophy. Muscle Nerve 2001;24:826–9.
[9] Fidzianska A, Hausmanowa-Petrusewicz I. Architectural abnormalities in muscle nuclei. Ultrastructural differences between X-linked and autosomal dominant forms of EDMD. J Neurol Sci 2003;210:47–51.
[10] Fidzianska A, Glinka Z. Nuclear architecture remodelling in envelopathies. Folia Neuropathol 2007;45:47–55.
[11] Nonaka I, Satoyoshi E. Myotonic dystrophy. In: Mastalgia F, Walton L, editors. Skeletal muscle pathology. 2nd ed. Edinburgh: Churchill Livingstone; 1992. p. 319–42.
[12] Bione S, Maestrini E, Rivella S, et al. Identification of a novel X-linked gene responsible for Emery-Dreifuss muscular dystrophy. Nat Genet 1994;8:323–7.
[13] Gruenbaum Y, Margalit A, Goldman RD, Shumaker DK, Wilson KL. The nuclear lamina comes of age. Nat Rev Mol Cell Biol 2005;6:21–31.
[14] Taniura H, Glass C, Gerace L. A chromatin binding site in the tail domain of nuclear lamins that interacts with core histones. J Cell Biol 1995;131:33–44.
[15] Ozawa R, Hayashi YK, Ogawa M, et al. Emerin-lacking mice show minimal motor and cardiac dysfunctions with nuclear-associated vacuoles. Am J Pathol 2006;168:907–17.
[16] Bakay M, Wang Z, Melcon G, et al. Nuclear envelope dystrophies show a transcriptional fingerprint suggesting disruption of Rb-MyoD pathways in muscle regeneration. Brain 2006;129:996–1013.
[17] Frock RL, Kudlow BA, Evans AM, Jameson SA, Hauschka SD, Kennedy BK. Lamin A/C and emerin are critical for skeletal muscle satellite cell differentiation. Genes Dev 2006;20:486–500.
[18] Hawke TJ, Garry DJ. Myogenic satellite cells: physiology to molecular biology. J Appl Physiol 2001;91:534–51.
[19] Olguin HC, Yang Z, Tapscott SJ, Olwin BB. Reciprocal inhibition between Pax7 and muscle regulatory factors modulates myogenic cell fate determination. J Cell Biol 2007;177:769–79.
[20] Yamane A, Akutsu S, Diekwisch TG, Matsuda R. Satellite cells and utrophin are not directly correlated with the degree of skeletal muscle damage in mdx mice. Am J Physiol Cell Physiol 2005;289:C42–48.

Original Paper

European Neurology

Eur Neurol 2009;62:304–310
DOI: 10.1159/000235943

Received: December 19, 2008
Accepted: July 13, 2009
Published online: September 3, 2009

Long-Term Prognosis of Patients with Large Subcortical Infarctions

Yutaka Suto[a] Hiroyuki Nakayasu[b] Masanobu Maeda[a] Masayoshi Kusumi[a]
Hisanori Kowa[a] Etsuko Awaki[c] Jun Saito[d] Kenji Nakashima[a]

[a]Department of Neurology, Institute of Neurological Sciences, Faculty of Medicine, Tottori University, Yonago, [b]Department of Neurology, Tottori Prefectural Central Hospital, Tottori, [c]Department of Neurology, Saiseikai Sakaiminato General Hospital, Sakaiminato, and [d]Department of Neurology, Shimane Prefectural Central Hospital, Izumo, Japan

Key Words
Prospective study · Ischemic stroke · Branch atheromatous disease

Abstract
Aim: We assessed the long-term prognosis of patients with large subcortical infarctions (LSCI). ***Methods:*** We defined LSCI as lesions ≥15 mm confined to deep penetrating arteries without a cardioembolic or atherothrombotic source. Patients with acute ischemic strokes were consecutively registered and followed for 751 ± 441 days. The clinical characteristics and long-term prognoses of patients with LSCI were compared to those of patients with lacunar (LACI), atherothrombotic (ATI) and cardioembolic infarctions (CEI). ***Results:*** At discharge from the hospital, the proportion of good outcomes (modified Rankin Scale ≤2) for patients with LSCI (52.1%) was similar to that for ATIs (47.2%), but worse than that for LACIs (73.2%). After a 3-year follow-up period, the mortality rates from LSCI, LACIs, ATIs and CEIs were 8.4, 8.2, 22.3 and 41.1%, respectively; the recurrence rates were 9.3, 14.1, 16.6 and 23.8%, respectively. ***Conclusions:*** The short-term prognosis of functional outcomes for LSCI was worse than that for LACIs, but similar to acute-phase ATI outcomes. The long-term prognosis after a LSCI is good, and recurrence tends to be lower than for LACIs.

Introduction

Infarctions with diameters ≥15 mm located in deep penetrating arteries are called giant lacunae or LSCI [1, 2]. In clinical practice, patients with LSCI who present with progressive stroke conditions (stroke-in-evolution) in the acute phase are encountered frequently. The presence of a LSCI is becoming increasingly important, despite the relatively small number of patients identified with the condition and the lack of clear clinical characteristics. A considerable number of LSCI show no apparent cardioembolic source or occlusion of major arteries. These types of LSCI are usually classified as giant lacunae, based on the criteria of the National Institute of Neurological Disorders and Stroke [3], or as 'strokes of undetermined etiology', based on the criteria of the Trial of Org 10172 in Acute Stroke Treatment [4]. The clinical characteristics of this condition, including the long-term prognosis, remain unclear. Therefore, understanding the pathobiology and etiology of LSCI may benefit patients who remain disabled as a result of these infarction events.

Two reports have described the long-term prognosis following LSCI [1, 5]. Donnan et al. [5] found that the rate of recurrent stroke or vascular death following a LSCI is approximately 2.7% per year during a mean follow-up

KARGER
Fax +41 61 306 12 34
E-Mail karger@karger.ch
www.karger.com

0014–3022/09/0625–0304$26.00/0

Accessible online at:
www.karger.com/ene

Yutaka Suto
Department of Neurology, Institute of Neurological Sciences
Faculty of Medicine, Tottori University
36-1 Nishi-cho, Yonago 683-8504 (Japan)
Tel. +81 859 38 6757, Fax +81 859 38 6759, E-Mail sutou@med.tottori-u.ac.jp

period of 2.25 years. Halkes et al. [1] concluded that the rate of recurrence in patients with large subcortical infarcts (21%) does not differ from that in patients with cortical infarcts (22%) or small, deep infarcts (19%) after an average follow-up of 9.2 years in patients who had a transient or minor ischemic attack. No reports have described the long-term prognosis of LSCI compared with that of lacunar (LACI), atherothrombotic (ATI) or cardiogenic infarctions (CEI). Clarification of the long-term prognosis for patients with LSCI would be useful for prediction of death or recurrence of a cerebral infarction. Therefore, the purpose of this study was to determine the 3-year prognosis of patients with LSCI and compare outcomes for this type of stroke with those for other subtypes.

Subjects and Methods

Patients were registered in the Tottori University Lacunar Infarction Prognosis Study [6]. This study, started in 1999, was a collaborative effort with 3 central hospitals and 1 university hospital in the San-In district of western Japan. A total of 1,460 Japanese patients with acute ischemic strokes were consecutively registered over 3.5 years from December 1999 to May 2003. An acute ischemic stroke was defined as an infarction within 14 days of onset of symptoms. The mean period from stroke onset to admission was 1.5 days. Transient ischemic attacks were excluded from the registry. Registration data were gathered and statistically analyzed in the Department of Neurology at Tottori University.

Details gathered at registration included the following: gender; age; clinical conditions; brain imaging [head computed tomography (CT) and magnetic resonance imaging (MRI)]; intracranial vascular examinations [magnetic resonance angiography (MRA), 3-dimensional CT and angiography]; extracranial vascular examination (carotid ultrasonography); cardiac examinations [electrocardiography (ECG), transthoracic echocardiography and transesophageal echocardiography (TEE)]; determination of risk factors (hypertension, diabetes mellitus, dyslipidemia, smoking, heavy alcohol consumption and previous history of stroke); use of therapeutic medications (antiplatelet and anticoagulant therapy), and activities of daily living, assessed with the modified Rankin Scale (mRS) at hospitalization and discharge from the hospital.

Registration data were categorized according to specific criteria. Progression was defined as the presence of progressive clinical deficits or gradual deterioration after stroke onset. Progression was determined by neurologists at each facility. Risk factors have been described in detail previously [6]. Patients who were taking antiplatelet drugs or anticoagulants at the time of discharge from hospital were considered to be 'receiving treatment'. Antiplatelet drugs included aspirin, ticlopidine, cilostazol, dipyridamole, ibudilast, ifenprodil and nicergoline. At the time of this study, clopidogrel and dipyridamole had not been approved in Japan for treatment of ischemic stroke. Therapeutic drugs were administered at the discretion of the neurologist at each facility.

The specific examinations conducted were as follows: head CT, 1,460 cases (100%); MRI, 1,298 cases (88.9%); 3-dimensional CT, 22 cases (1.5%); angiography, 33 cases (2.3%); carotid ultrasonography, 1,181 cases (80.9%); ECG, 1,441 cases (98.7%); transthoracic ultrasonography, 1,103 cases (75.5%), and TEE, 101 cases (6.9%). Holter ECG monitoring was also performed in almost the same number of cases as TEE. Lesion size was investigated using diffusion-weighted imaging (DWI), T2-weighted imaging or fluid-attenuated inversion recovery (FLAIR) imaging (88.9%) or CT (11.1%). The mean duration from onset to imaging studies was less than 7 days.

Subtypes of ischemic stroke were classified according to the decision tree shown in figure 1 (modified from the National Institute of Neurological Disorders and Stroke Stroke Data Bank [3]). CEI was classified as an infarction with cardiogenic sources [4], based on the cardiac examinations. ATI was classified as an infarction lacking a cardioembolic source and with significant ($\geq$50%) stenosis or occlusion of the major arteries that supply the ischemic region, as observed via intra- or extracranial vascular examinations. LACI was classified as an infarction lacking a cardioembolic source and without significant ($\geq$50%) stenosis or occlusion of the major arteries that supply the ischemic region; these lesions were <15 mm in diameter in the subcortical or brainstem regions, as determined by imaging. LACI also included patients whose lesions were not revealed by imaging but who showed the classical lacunar syndrome as a clinical manifestation. Other brain infarctions of known etiology, consisting of infarctions caused by cerebral artery dissection or vascular inflammation, were excluded from the final analysis. Infarctions of uncertain cause (IUC) included those that could not be classified into one of the above categories. LSCI were defined as infarctions with a lesion $\geq$15 mm in diameter that was confined to one or a few penetrating branches in the subcortex or brainstem, without a cardioembolic source and without significant stenosis or occlusion of the major arteries that supply the ischemic region. The perfusion territories of the penetrating arteries were defined according to Tatu et al. [7, 8].

Follow-up continued until the patients dropped out of the study, died or could no longer be located. The mean duration of follow-up until death or dropout was 751 $\pm$ 441 days (median 1,095 days). Follow-up information was obtained from each participating research facility by a review of medical records, telephone surveys and mail-in surveys to the hospitals. Recurrence, subtype (if any) and cause of death (if any) were noted.

Statistical analyses were performed as follows. The χ^2 test was used to compare baseline characteristics, risk factors and therapeutic drug use. One-way analysis of variance was used to compare patient age and duration of hospitalization among the 4 stroke subtypes. Kaplan-Meier curves and log-rank tests were used to study mortality and recurrence rates among stroke subtypes. A Cox regression hazards model was used for stepwise multiple regression analysis. Values of $p < 0.05$ were considered to be statistically significant. All statistical analyses were performed using SPSS 15.0J software for Windows (SPSS Japan, Japan).

This study was conducted with the approval of Tottori University and the ethics committee at each participating institution.

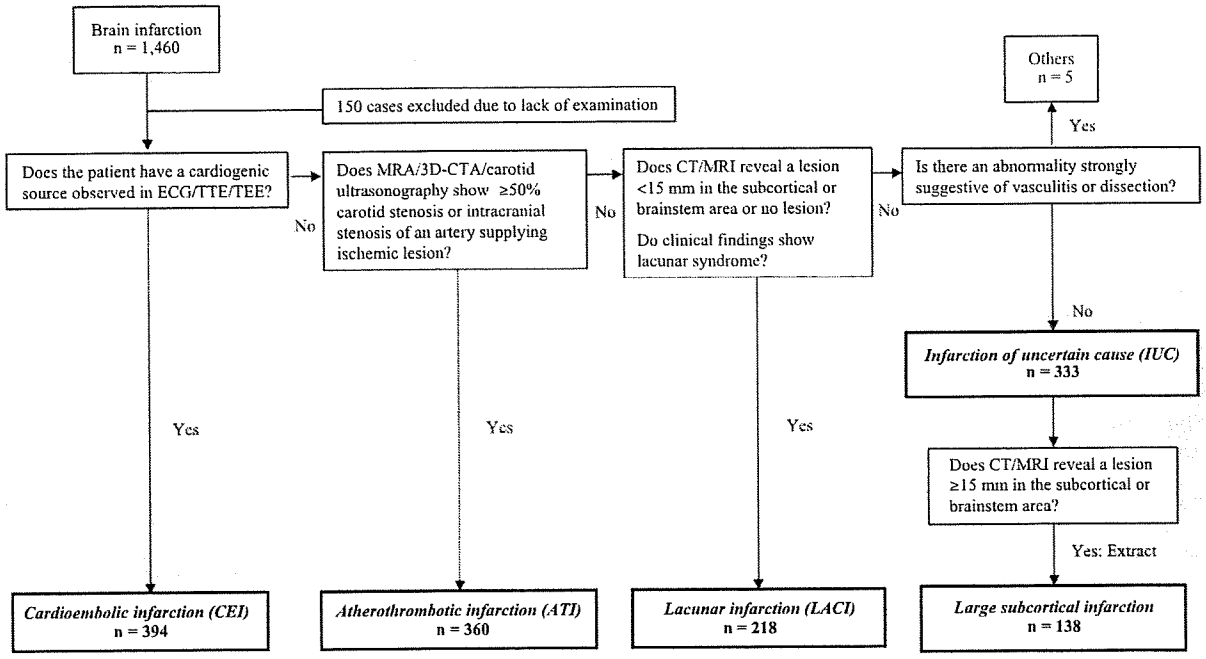

Fig. 1. Stroke classification (decision tree). TTE = Transthoracic echocardiography; 3D-CTA = 3-dimensional CT angiography.

Results

Among the 1,460 registered stroke cases, 150 cases could not be diagnosed due to insufficient data and were excluded. The remaining 1,310 cases were divided into 5 stroke subtypes (fig. 1). The frequencies of each subtype were as follows: CEI, 394 cases (27.0%); ATI, 360 cases (24.7%); LACI, 218 cases (14.9%); IUC, 333 cases (22.8%), and other brain infarctions of known etiology, 5 cases (0.3%). Careful analysis of the 333 IUC cases showed that 138 had LSCI (9.5%). These consisted of 109 infarcts located in the subcortex and 29 in the brainstem.

Baseline Characteristics of LSCI Compared to Other Subtypes

The baseline characteristics of the patients with LSCI are displayed in table 1. The majority of patients with LSCI were women. Compared to the other subtypes, the frequency of patients who had a history of stroke was lower, but the frequency with progressive temporal profiles at stroke onset was higher. Smoking was less frequent in patients with LSCI than in patients with ATIs or LACIs. Patients with LSCI showed a lower rate of disturbances in consciousness and cortical dysfunction compared with patients who had CEIs or ATIs. Regarding therapeutic drugs, 87.7% of patients with LSCI took antiplatelet drugs, similar to patients with ATIs or LACIs.

Short-Term Prognosis of LSCI

Short-term prognosis was assessed using the mRS at the time of hospitalization and discharge, taking into account the number of days spent in the hospital (table 1). Good outcomes (mRS ≤ 2) were seen for LACIs, LSCI, ATIs and CEIs, in descending order of frequency. Comparing the various subtypes by χ^2 tests, the proportion of good outcomes for LSCI (52.1%) was similar to that for ATIs (47.2%; $p = 0.67$), but was significantly worse than that for LACIs (73.2%; $p < 0.01$). In contrast, the proportion of deaths from LSCI (0.8%) was similar to that for LACIs (0%), but was better than that for ATIs (5.9%; $p < 0.01$). The duration of hospitalization for patients with LSCI was significantly lower than for ATIs and CEIs, but was significantly greater than for LACIs.